*Manuscript (with LINE NUMBERS)

Low-temperature thermochronology of the South Atlantic margin along Uruguay and its relation to tectonic events in West Gondwana

João Pacífico **Silveira Luiz Machado**[1,2]*, Andréa **Ritter Jelinek**[2], Randell **Stephenson**[1], Claudio **Gaucher**[3], Marcos **Müller Bicca**[2], Leticia **Chiglino**[3], Frederico Antonio **Genezini**[4]

[1] School of Geosciences, University of Aberdeen, United Kingdom

[2] Instituto de Geociências, Universidade Federal do Rio Grande do Sul, Porto Alegre, Brazil

[3] Facultad de Ciencias, Universidad de la República, Montevideo, Uruguay

[4] Instituto de Pesquisas Energéticas e Nucleares, Centro do Reator de Pesquisas, São Paulo, Brazil

* Correspondence (j.luizmachado.18@abdn.ac.uk / joao.machado@ufrgs.br)

Abstract

The geodynamic forces acting during Jurassic-Cretaceous South Atlantic rifting provoked intense transformations in West Gondwana, such as the reactivation of ancient basement structures, broad magmatism and general uplift of the new continental margins. Low-temperature thermochronology records cooling associated with exhumation syn- and post-breakup along the Brazilian margin, while further south, in Uruguay, mostly pre-breakup uplift is identified. Thermochronometry data are scarce in Uruguay, but previous studies suggest that basement cooling and exhumation preceded West Gondwana breakup by hundreds of millions of years. To improve our knowledge of the evolution of rifting, we present 19 apatite fission-track ages in this study, 42 apatite and 40 zircon (U-Th)/He single crystal ages for the Uruguayan shield (UYS), from which we modeled 19 inverse thermal histories. Our results suggest that the UYS temperatures were below 200 °C since the early Paleozoic, and that cooling below 110 °C started during the Carboniferous, with continuous exhumation of the basement until Early Cretaceous. The onset of this long-term uplift is correlated with orogenesis and terrane accretions in the SW margin of West Gondwana during the Paleozoic. Lithosphere thinning and uplift preceding breakup contributed to the continuous Late Paleozoic to middle Mesozoic exhumation, until the voluminous volcanism of the Paraná-Etendeka Large Igneous Province (*c.* 133 Ma). This magmatic event, combined with the thermal influence of the Tristão da Cunha mantle plume and rift spreading, likely raised the basement geotherm during the Late Cretaceous. Models suggest a slight increase in temperatures of the UYS from Late Cretaceous until the Oligocene, when a final cooling to surface temperatures took place. Our findings corroborate a long and complex thermal history for Uruguay, with crustal uplift occurring essentially before West Gondwana breakup.

Keywords

Thermochronometry; Fission-tracks; (U-Th)/He; West Gondwana; South Atlantic.

1. Introduction

The Atlantic passive margin in South America was established after Gondwana breakup in the Jurassic-Cretaceous, during which rifting propagated from southernmost Tierra del Fuego towards the NE, forming the eastern continental margins of Argentina, Uruguay and Brazil. Basement uplift and exhumation syn- and post-rift have been widely reported by low-temperature thermochronometry studies in SE Brazil (*e.g.* Gallagher *et al.* 1994, 1995; Gallagher & Brown 1999; Tello Saenz *et al.* 2003; Hackspacher *et al.* 2004; Cogné *et al.* 2011, 2012; Karl *et al.* 2013; Krob *et al.* 2019; Van Ranst *et al.* 2019), where the high escarpments (up to 2.000 m) from the Serra do Mar and Serra da Mantiqueira provide an ideal scenario for this research method. Cooling in the region is often associated with uplift and exhumation, related to the far-field effects of the Andean Orogeny and to structural reactivations in the passive margin during the development of the Atlantic Ocean. On the other hand, thermochronometry studies are scarcer towards the south of the Atlantic margin, where a subdued topography and low relief are dominant. Published data suggest that an important limit between pre- and post-rift cooling and exhumation is located in the Florianópolis region, southern Brazil (Fig. 1), where a very complex thermal history has been reported (Jelinek *et al.* 2003; Karl *et al.* 2013; Hueck *et al.* 2018a). Further south of this region, thermochronometry studies have reported mainly pre-rift Paleozoic cooling phases in southernmost Brazil (Borba *et al.* 2002, 2003; Oliveira *et al.* 2016; Machado *et al.* 2019), Uruguay (Kollenz 2015; Hueck *et al.* 2017; Gomes & Almeida 2019) and Argentina (Kollenz *et al.* 2017). These were generally linked to Paleozoic orogenic cycles on the active SW margin of Gondwana and the geodynamics of Gondwana breakup.

Approximately 800 km south of Florianópolis, Uruguay has represented an area of increased interest for thermochronometry studies in recent years, but data are still very limited in the region. The Uruguayan shield (UYS) occupies almost half of the territory of Uruguay (Fig. 1 and 2) and includes exposures of the Archean to Paleoproterozoic Rio de La Plata Craton and of the Neoproterozoic Dom Feliciano Belt, associated with the formation of West Gondwana (Hartmann *et al.* 2001; Gaucher *et al.* 2011; Oyhantçabal *et al.* 2011). Although passive margins and cratons are often considered as characterized by long-term stability, the low-temperature thermochronology studies in Uruguay indicate basement cooling since the early Paleozoic, suggesting a lengthy and complex Phanerozoic thermotectonic history. Available data suggest that the main exhumation event in the region was initiated well before Gondwana breakup (Kollenz 2015; Hueck *et al.* 2017; Gomes & Almeida 2019). However, the current thermal histories modeled for the UYS by different authors and based on distinct thermochronometers (Kollenz 2015; Hueck *et al.* 2017; Gomes & Almeida 2019) suggest alternative phases of cooling and reheating of the basement, and imply conflicting geodynamic models for the regional tectonic evolution. The complex and scattered thermochronometry data in the region represent a restraint to our understanding of the tectonic activity preceding South Atlantic rifting and breakup.

A deeper comprehension of the cooling and exhumation history of the Uruguay basement can improve our models for the Gondwana breakup and tectonic activity in the early stages of rifting, including rift propagation northwards. Moreover, it is necessary to evaluate the somewhat conflicting models for exhumation of the UYS. Therefore, with the objective to enhance our knowledge of the thermal history of the region, in this work we combine the methods used individually in previous thermochronometry studies and generate new thermal models for the Uruguayan basement. We present a new dataset with 19 apatite fission-track ages, 42 apatite and 40 zircon (U-Th)/He single crystal ages, from which we model 19 inverse thermal histories across the UYS. After integration with previously published data, we identify the main cooling/reheating phases of the shield and associate them to the collisional cycles in the SW margin of Gondwana, and to the opening of the South Atlantic. Our results support models of a complex long-lived thermal evolution for the Uruguayan shield, and a thermotectonic history that utilizes the thermochronometry data currently available for the region is suggested.

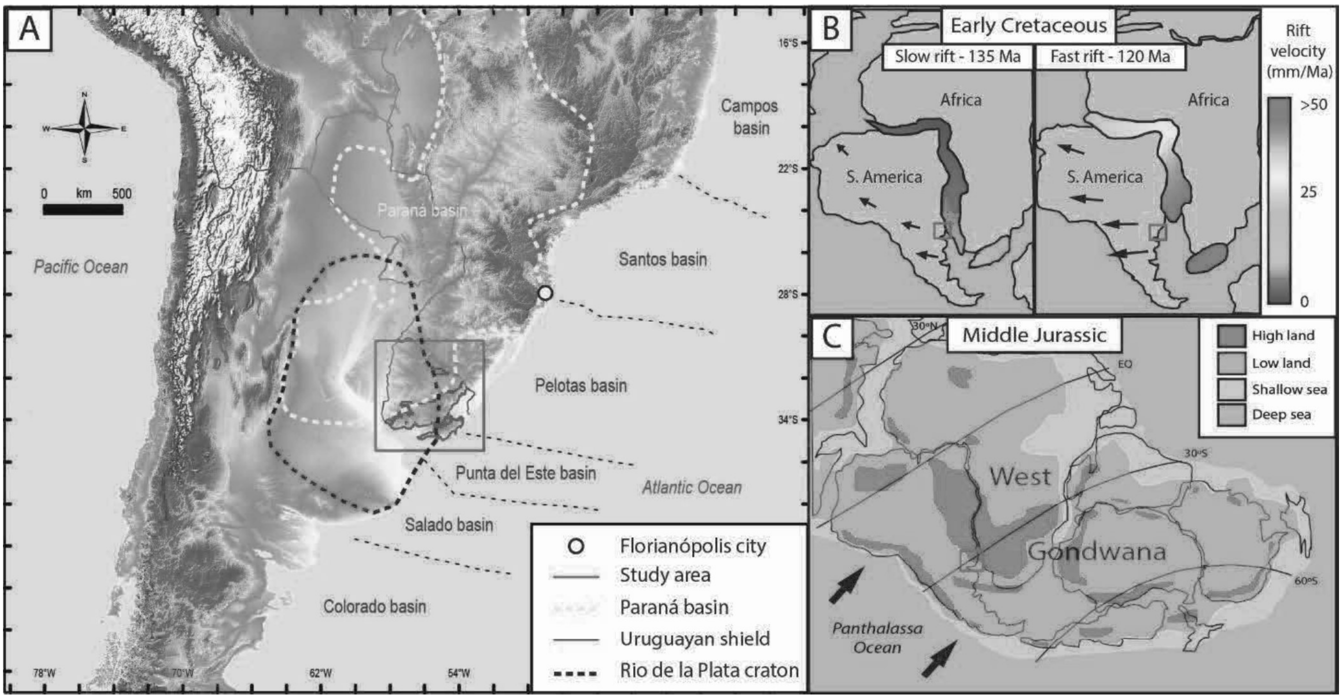

Figure 1. Panel with (A) DEM image of the study area in the South Atlantic margin, with schematic boundaries of the Paraná Basin and Rio de La Plata Craton indicated. The region of Florianópolis marks the limit between pre-rift cooling (south) and post-rift cooling (north); (B) study area location during the South Atlantic rift velocity increase (after Brune et al., 2016) and (C) before West Gondwana break-up, with subduction of the Panthalassa Ocean under West Gondwana (after Scotese et al., 1999).

2. Geological context

Uruguay is located at the eastern margin of South America and exhibits a surprising geological diversity considering its relatively small size (176.215 km^2). Its Precambrian basement records geological events from the Archean, accessible to investigation by exposure across 44% of its territory (Bossi *et al.* 1998; Hartmann *et al.* 2001; Masquelin 2006). The country has low topography and subdued relief, with very few peaks over 500 m above sea level. The Uruguayan shield crops out mainly in the southern and eastern part of the country, and is divided into four tectonostratigraphic terranes, while the remaining area is covered by Phanerozoic volcano-sedimentary deposits (Fig. 2).

2.1 The Uruguayan shield (UYS)

The four UYS terranes are limited by regional shear zones and known, from W to E, as the: 1) Piedra Alta Terrane (PAT), 2) Tandilia Terrane (TT), 3) Nico Pérez Terrane (NPT), and 4) Cuchilla Dionisio Terrane (CDT) (Bossi *et al.* 1998; Bossi & Gaucher 2004, 2014a; Bossi & Cingolani 2009). Although this division is still a matter of debate, the westernmost PAT and TT are unanimously considered part of the Rio de la Plata Craton, a major tectonic feature in South America; the easternmost CDT represents the Dom Feliciano Belt and had been associated with the Kalahari Craton, of southern Africa; and the central and highly complex NPT has been considered part of the Rio de La Plata Craton or not, depending on author (see Basei et al., 2005; Bossi and Gaucher, 2004; Gaucher et al., 2011; Hartmann et al., 2001; Masquelin, 2006; Oriolo et al., 2016a; Oyhantçabal et al., 2018; Philipp et al., 2016; Rapela et al., 2011; Santos et al., 2017). In any case, there is consensus that all terranes were finally assembled during the end of the Brasiliano/Pan-African Orogeny (Neoproterozoic), a multi-episodic collision between the Rio de la Plata, Congo and Kalahari cratons and several microcontinents and arc terranes (e.g. Arachania), which culminated with the consolidation of West Gondwana (Gaucher *et al.* 2009, 2011; Hueck *et al.* 2018b; Philipp *et al.* 2018; Schmitt *et al.* 2018a).

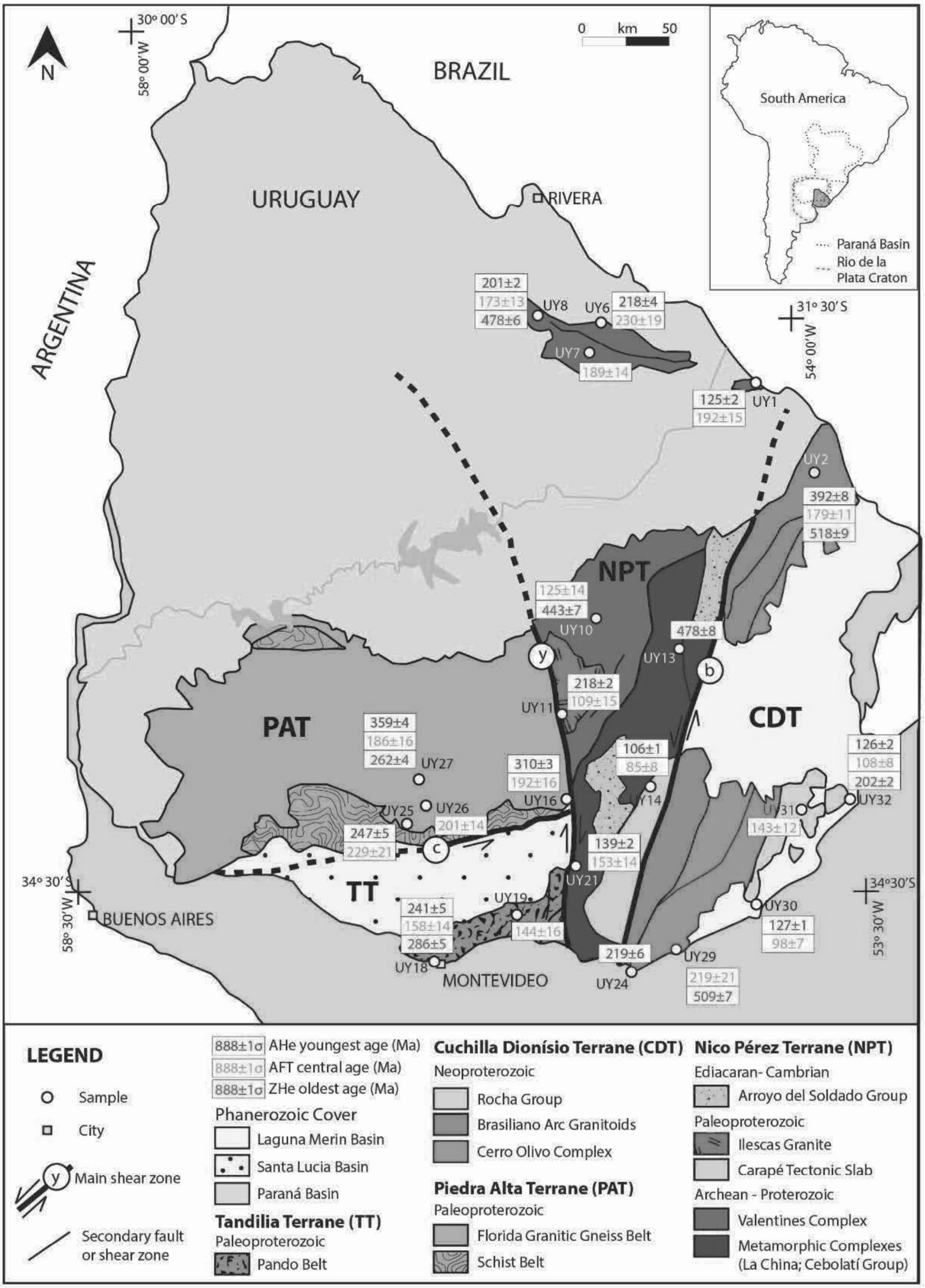

Figure 2. Simplified geological map of Uruguay with sample locations and new thermochronometry ages. Central AFT ages, oldest ZHe and youngest AHe single crystal ages are reported. Main shear zones: (c) Colonia, (y) Sarandí del Yí and (b) Sierra Ballena. Inset map indicates the approximated extension of the Paraná Basin and Rio de la Plata Craton.

Three major crustal-scale regional shear zones delimit the four UYS terranes, and several NE-trending smaller lineaments occur in the NPT and CDT. The oldest lineament is the Colonia Shear Zone, which separates the PAT from the TT (Bossi and Cingolani, 2009). It comprises an E-W trending, several km-thick ultramylonite band showing abundant sinistral shear indicators (Ribot et al., 2005; Abre et al., 2014). The age of the shear zone has been determined by K-Ar ages of deformed granitoids as 1.75 Ga (Faraone, 2018). Central in the shield, the Sarandí del Yí Shear Zone is a mylonitic belt with *c.* 2 km width and a NNW-SSE strike, which displays dextral shearing with sinistral reactivation and limits the western PAT and TT from the central NPT (Bossi & Gaucher 2014a; Oriolo *et al.* 2018). Ar-Ar ages of mafic dikes deformed by the main dextral shear yielded Mesoproterozoic ages of *c.* 1,200 Ma (Teixeira et al., 1999), that were related to the tangential collision between the TPA and TT with the NPT during the formation of the Rodinia supercontinent (Bossi & Cingolani 2009; Gaucher *et al.* 2011; Bossi & Gaucher 2014a). More recent publications have supported a Neoproterozoic onset of deformation (*c.* 630 Ma), linked to the collision of the Rio de la Plata and Congo cratons during West Gondwana formation (Rapela *et al.* 2011; Oriolo *et al.* 2016b, 2018), but the new ages do not rule out a Mesoproterozoic main event (Santos et al., 2017). This discussion is still ongoing and has important implications for the Precambrian evolution of Uruguay. Another major lineament is the Sierra Ballena Shear Zone, a *c.* 4 km-wide mylonitic belt with NNE-SSW direction that propagates to southernmost Brazil as the Dorsal do Canguçu Shear Zone (Fernandes *et al.* 1993; Fernandes & Koester 1999; Oriolo *et al.* 2018). In Uruguay this shear zone represents the suture between the central NPT and the coastal CDT, and displays sinistral shearing during the end of the Brasiliano/Pan-African Orogeny (latest Ediacaran-Cambrian) with brittle reactivation during the Mesozoic (Bossi & Gaucher 2004, 2014a; Hueck *et al.* 2017; Oriolo *et al.* 2018).

The PAT is a Paleoproterozoic (2.2 to 2.0 Ga) block composed of two supracrustal low-grade metamorphic belts (Arroyo Grande and San José belts), separated by the wide central Florida Belt, which comprises granitoids and gneiss (Hartmann *et al.* 2001; Oyhantçabal *et al.* 2011; Bossi & Piñeyro 2014). The southern San José Belt is cut by the E-W Colonia Shear Zone and partially covered by the Santa Lucía Basin. The central Florida Belt was intruded by thousands of mafic dikes with E-W direction around 1.79 Ga (Teixeira *et al*., 1999) which underwent a NW-SE flexure near the Sarandí del Yí Shear Zone, indicating dextral movement during the collision of the PAT and the NPT (Bossi and Campal, 1992; Hartmann *et al.* 2001; Gaucher *et al.* 2011; Bossi & Piñeyro 2014; Oriolo *et al.* 2016b; Oyhantçabal *et al.* 2018). The PAT yielded widespread positive εNd values and Nd model ages between 2.4 and 2.1 Ga, which shows its juvenile character and lack of an Archean basement (Pamoukaghlián et al., 2017).

The TT, to the south of the Colonia Shear Zone, comprises the Paleoproterozoic Montevideo Formation (Pando Belt) and several intrusive granitoids, such as the Soca rapakivi granite (2056 Ma: Santos et al., 2003) and the La Tuna Granite, which yielded a U-Pb crystallization age of 2156 Ma (Pamoukaghlián et al., 2017). The terrane continues to the south beneath the Río de la Plata and into Argentina, cropping out again in its type area (Tandilia) in the southern Buenos Aires Province, Argentina (Bossi and Cingolani, 2009). Apart from older ages for the metasediments and intrusive granitoids compared to the PAT, Nd model ages are in average 200 Myr older in the TT (Pamoukaghlián et al., 2017), matching comparable model ages in the type area in Argentina (Hartmann et al., 2002). Furthermore, Neoproterozoic anorogenic granitoids and sedimentary rocks occur in the TT in Argentina and Uruguay (Gaucher et al., 2008; Abre et al., 2014) but are so far unknown in the PAT.

The NPT (Bossi and Campal, 1992; Bossi *et al.* 1998) is a complex terrane in Uruguay and a key element for understanding the formation of West Gondwana. It is usually considered part of the Rio de la Plata Craton since the Mesoproterozoic (Hartmann *et al.* 2001; Gaucher et al., 2008, 2009b; Bossi & Cingolani 2009; Santos *et al.*, 2017), but other studies have related the NPT to the Congo Craton, suggesting it was amalgamated to the Rio de la Plata Craton only during the Ediacaran (Oyhantçabal *et al.* 2011; Rapela *et al.* 2011; Oriolo *et al.* 2016a). The NPT presents a highly complex geology and the oldest rocks in Uruguay, with major internal units limited by the NE-SW shear zones, a basement window (Isla Cristalina de Rivera) cropping out far north in the Paraná Basin (Fig. 2), and continuity to southernmost Brazil (Taquarembó Terrane) (Oyhantçabal *et al.* 2011, 2012; Bossi & Gaucher 2014b; Oriolo *et al.* 2016a, 2018). In a simplified way, the NPT is composed of the Valentines Granulitic Complex in the northwest, the La China Complex and the Cebolatí Group in the middle, and the Carapé Tectonic Slab and Mesoproterozoic volcano-sedimentary successions in the southeast. The Valentines Complex, which includes the Isla Cristalina de Rivera, comprises gneisses (felsic granulites), pyroxenites and banded iron formations (BIF) as well as intruding tonalites, trondhjemites and granites with ages between 2.6 and 2.2 Ga (Santos et al., 2003; Oyhantcabal et al., 2012). They are in turn intruded by the Illescas rapakivi granite, which yielded an U-Pb zircon age of 1.784 Ma (Bossi *et al.* 1998; Bossi & Cingolani 2009). The central domain includes the La China Complex, which comprises metatonalites of amphibolite facies, and the metasedimentary Cebollatí Group (formerly known under the informal term "Las Tetas complex"), both units with Archean ages between 3.4 and 2.7 Ga (Hartmann *et al.* 2001; Gaucher *et al.* 2010, 2011, 2014b). To the southeast of the Archean units, a NE-trending belt of Mesoproterozoic (1.5-1.3 Ga), low-grade meta-volcano-sedimentary rocks occurs, which includes the Parque UTE and Mina Verdún groups and the Tapes Complex (Chiglino et al., 2010; Gaucher et al., 2011, 2014a;

Poiré et al., 2005). At the southeastern corner of the NPT, the Carapé Complex, sometimes referred to as the Campanero Unit, is a tectonic slab emplaced in the NPT in the latest Ediacaran-early Cambrian, and comprises mainly metagranitoids and metasediments juxtaposed by reverse and transcurrent faults (Hartmann *et al.* 2001; Mallmann *et al.* 2007; Chiglino *et al*. 2010, Bossi *et al.* 2014). Unconformably overlying parts of the NPT are remnants of the Arroyo del Soldado Group, a 5,000 m thick marine platform succession rich in carbonate deposits and with depositional age between 566 and 530 Ma (Gaucher, 2000; Gaucher *et al.* 2004; Blanco *et al.* 2009).

The CDT, also known as Punta del Este Terrane (Oyhantçabal *et al.* 2011), is an allochthonous unit laterally accreted to the NPT during the Brasiliano/Pan-African Orogeny (Bossi & Gaucher 2004). This terrane is composed mainly of deformed calc-alkaline granitic (e.g. Aiguá and Cuchilla Dionisio batholiths) with ages between 615 and 530 Ma, and occupies most of the CDT and is known in Brazil as the Pelotas Batholith (Fernandes *et al.* 1995; Bossi & Gaucher 2004; Philipp *et al.* 2016). The Paleo-Mesoproterozoic Cerro Olivo Complex occurs further east; it is considered the basement of this terrane and includes high-grade metamorphic rocks with protolith ages between 1000 and 750 Ma, metamorphosed at *c.* 650 Ma (Bossi & Gaucher 2004; Basei *et al.* 2011; Oyhantçabal *et al.* 2011; Peel *et al*. 2018; Will *et al*. 2019). Finally, near the South Atlantic coast the metasediments of the Rocha Group, are exposed. These have ages between *c.* 600 to 550 Ma and affinity to units from the Kalahari Craton, being correlated to the Oranjemund Group of the Gariep Belt in Namibia (Bossi & Gaucher 2004; Basei *et al.* 2005).

Although the discussion is still ongoing on how and when the tectonostratigraphic terranes of the UYS were assembled, there is a consensus that the long lived Brasiliano/Pan-African Orogeny represents the final event for the consolidation of Uruguayan basement. The juxtaposition of UYS terranes, related to the diachronous collision of Uruguayan, Brazilian and African units, led to the formation of the West Gondwana megacontinent by Cambrian times (Bossi & Gaucher 2004, 2014a). The successive collisions related to the Brasiliano/Pan-African Orogeny were responsible for establishing sutures that later played an important role during Pangea breakup and South Atlantic opening in the Mesozoic (Oriolo *et al.* 2018; Schmitt *et al.* 2018; Will & Frimmel 2018).

2.2 Phanerozoic cover

Most of the territory of Uruguay is covered by remnants of three Phanerozoic basins: the continentally wide intracratonic Paraná Basin, locally named the Norte Basin, and the relatively small and South Atlantic rift related Laguna Merin and Santa Lucia basins (Fig. 2).

The Paraná Basin, which spreads over Argentina, Brazil, Paraguay and Uruguay, was developed in the interior of West Gondwana during Paleozoic and Mesozoic times. Depositional packages within this basin are divided into six supersequences separated by interregional unconformities: Rio Ivaí (Ordovician to Silurian), Paraná (Devonian), Gondwana I (Upper Carboniferous to Lower Triassic), Gondwana II (Middle to Upper Triassic), Gondwana III (Jurassic to Lower Cretaceous), and Bauru (Upper Cretaceous) (Milani 1997; Milani *et al.* 2007). The SE margin of the Paraná Basin lies within Uruguay (Fig. 1), where basinal deposits cover most of the NW of the country and are associated with the supersequences Paraná, Gondwana I and Gondwana III, reaching a maximum thickness between 2,300 and 3,000 m (de Santa Ana *et al* 2006). The lowermost deposits correspond to the Durazno Group, cropping out at the SE margin of the basin and related to the Paraná Supersequence. This group comprises a transgressive-regressive siliciclastic sequence of shallow marine deposits, with paleocurrents to the NW and sourced from the UYS terranes, being deposited within an extensional subsidence regime (Sprechmann *et al*. 1993; Uriz *et al.* 2016). Separated by an unconformity, the overlying depositional sequence Gondwana I Supersequence represents a transgressive-regressive cycle as well. It comprises latest

Carboniferous to Permian deposits that record the transition from glaciolacustrine, to marine and finally fluvial and aeolian environments (de Santa Ana *et al.* 2006; Beri *et al.* 2011). Last, unconformably above these, lies the continental deposits of the Gondwana III Supersequence, which comprises fluvial and aeolian formations capped by basalt flows from the Paraná-Etendeka Large Igneous Province (LIP) (Sprechmann *et al.*, 1981), with eruption peak at *c.* 133 Ma and related to the Tristão da Cunha mantle plume and the opening of the South Atlantic (Turner *et al.* 1994; Rossetti *et al.* 2014; Cernuschi *et al.* 2015).

The tectonic stress associated with Pangea breakup and Atlantic opening led to the development of the Santa Lucia and Laguna Merin basins onshore (Bossi *et al.* 1998), which form a ENE-WSW corridor known as SaLAM, that is considered an aborted rift precursor to the opening of the South Atlantic during the Jurassic-Cretaceous (Rossello *et al.* 2000). Despite the genetic link, the basins present distinct volcano-sedimentary infill and are separated by the NPT, where only smaller rift basins are found (Rossello *et al.* 2000). The SaLAM was formed during extensional tectonics related to Pangea breakup, with a later dextral transtensive phase associated by (Rossello *et al.* 2000, 2007) with the drifting movement that led to the completion of South Atlantic opening. The Santa Lucia Basin corresponds to the SW part of the SaLAM, presents a central structural high with E-W strike and comprises mostly siliciclastic deposits, reaching a total thickness of 2,500 m (Rossello *et al.* 2000; Veroslavsky *et al.* 2004). The NE SaLAM is represented by the Laguna Merin Basin, which is mainly composed of volcanic rocks with ages between 134 to 127 Ma and covered by Cenozoic sedimentary rocks (Cernuschi *et al.* 2015). The youngest volcanic rocks so far described in Uruguay are subalkaline rhyolites in southern NPT, dated U-Pb SHRIMP by Gaucher et al. (2016) at 77 ± 1 Ma (Campanian, Late Cretaceous).

3. Materials and methods

3.1 Sampling

For this study we collected basement samples from 32 outcrops across Uruguay. We avoided locations with published low-temperature thermochronometry data and aimed to cover most of the shield, collecting samples from the margins and central parts of each tectonostratigraphic terrane. Standard crushing, magnetic and heavy liquids separation were processes applied to separate apatite and zircon crystals. Although we sampled mainly granitic rocks, which are usually rich in apatite and zircon, only 21 samples provided crystals suitable for the thermochronometry analysis (Fig. 2, Tab. 1).

Sample	Lithology	Age (Ma)	Lat (°)	Long (°)	Altitude (m)	D. sea (km)	Analysis
UY1	Granite	> 550	-31.89	-54.16	225	181	AFT, AHe
UY2	Granite	575 ± 14	-32.35	-53.79	110	133	AFT, AHe, ZHe
UY6	Granite	590 - 530	-31.59	-55.10	259	277	AFT, AHe
UY7	Granite	550 - 510	-31.75	-55.18	208	278	AFT
UY8	Granite	590 - 530	-31.55	-55.49	193	312	AFT, AHe, ZHe
UY10	Granite	> 1000	-33.12	-55.13	245	173	AFT, ZHe
UY11	Granite	1785 ± 9	-33.61	-55.33	235	161	AFT, AHe
UY13	Granite	> 1000	-33.28	-54.62	102	120	ZHe
UY14	Granite	590 - 530	-33.99	-54.78	131	89	AFT, AHe
UY16	Granite	*c.* 2200	-34.06	-55.31	266	104	AFT, AHe
UY18	Gnaisse	*c.* 2200	-34.92	-56.17	150	111	AFT, AHe, ZHe
UY19	Granite	2054 ± 11	-34.67	-55.64	55	69	AFT
UY21	Granite	574 ± 34	-34.41	-55.25	182	66	AFT, AHe
UY24	Gnaisse	1006 ± 37	-34.97	-54.95	9	0	AHe
UY25	Diorite	2065 ± 9	-34.19	-56.32	54	153	AFT, AHe
UY26	Granite	*c.* 2100	-34.10	-56.20	47	150	AFT
UY27	Granite	*c.* 2200	-33.96	-56.24	133	163	AFT, AHe, ZHe
UY29	Granite	> 550	-34.85	-54.63	7	0	AFT, ZHe
UY30	Schist	< 1540	-34.59	-54.12	3	0	AFT, AHe
UY31	Granite	556 ± 7	-34.11	-53.85	71	17	AFT
UY32	Granite	678 ± 14	-34.04	-53.54	4	0	AFT, AHe, ZHe

Table 1: Details of each location and analysis made. Stratigraphic ages from Bossi & Gaucher (2004) and Masquelin (2006); coordinates in degrees and datum WGS84; (D. sea) is the shortest distance to the Atlantic Ocean.

3.2 Low-temperature thermochronometry

We used three low-temperature thermochronometers to investigate the thermal evolution of the Uruguayan basement: apatite fission-tracks (AFT), apatite (U-Th)/He (AHe) and zircon (U-Th)/He (ZHe). These radio-isotopic systems have distinct retention temperatures, and together cover an interval between *c.* 40 to 190 ºC, simply put, shallow crust temperatures. Each method has its specific partial retention zone (PRZ), which corresponds to a temperature interval where accumulation and loss of the radiogenic decay product are coeval. Temperatures lower than the PRZ of the thermochronometer appraised imply total retention of the radiogenic products, while higher temperatures than the PRZ result in complete loss of them, resetting the age of the thermochronometer to zero. Therefore, the age obtained by thermochronometry methods is a cooling age, based on the balance between radiogenic parent and decay product, and represents a time-temperature point during the passage through the PRZ of the thermochronometer.

Apatite fission-tracks thermochronometry is based on the accumulation of linear defects (tracks) in the crystal lattice, formed by spontaneous fission of ^{238}U and which the quantity and variable lengths indicates the thermal path experienced by the crystal (Price & Walker 1963; Fleischer *et al.* 1975; Gleadow *et al.* 1986a, b; Galbraith *et al.* 1990). The apatite fission-track partial retention zone (AFTPRZ) corresponds to temperatures between *c.* 60 to 110°C, in which the tracks slowly shrink in a process known as annealing (Wagner *et al.* 1989). Below *c.* 60°C the annealing process is not effective, and tracks are preserved with their full initial length (*c.* 16μm). Although temperature is the main factor controlling annealing, this process is also affected by variations in apatite chemical composition and the amount of accumulated radiation damage (Gleadow *et al.* 1986a; Stockli 2005; Tagami & O'Sullivan 2005).

We used the external detector method for AFT dating (Gleadow 1981; Hurford 1990). For each sample, more than 200 apatites were hand-picked and mounted in epoxy resin tablets, polished to the central portion, and etched in a 5.5M HNO3 solution at 21°C for 20 s to reveal the spontaneous fission tracks (Carlson *et al.* 1999). Muscovite sheets were coupled to the tablets, which then were irradiated at the IEA-R1/IPEN-CNEN Reactor, São Paulo, Brazil, along with Durango age standards and Corning CN5 dosimeters. Afterwards, mica sheets were decoupled and etched in 48% HF for 18 min at 20°C to reveal the induced tracks. AFT analyses were performed at the Universidade Federal do Rio Grande do Sul, Brazil, using a Leica DM 6000 M Microscope (1000x, dry). Ages were calculated based on 20 crystals per sample and the ζ calibration method (Hurford & Green 1983; Hurford 1990), while ages homogeneity was analyzed through the chi-square test (Galbraith 1981; Galbraith & Green 1990) using the software RadialPlotter 9.0 (Vermeesch 2009). For thermal modeling we aimed to measure lengths and *c*-axis angles of 100 confined TINT tracks (Lal *et al.* 1969) in each sample, and used the mean etch pit diameter D_{par} from about 100 measurements as kinetic parameter (Donelick 1993; Carlson *et al.* 1999; Donelick *et al.* 2005).

The (U-Th)/He method is based in the accumulation of alpha particles (^{4}He) in the crystal lattice after the decay chain of ^{238}U, ^{235}U and ^{232}Th isotopes. The alpha particles are expelled from the mineral structure at high temperatures owing to thermal diffusion. In apatite (U-Th)/He dating, alpha particles are efficiently expelled at temperatures above *c.* 70°C, partially retained between *c.* 40 and 70°C (AHe Partial Retention Zone – AHePRZ), and completely retained when temperature is below *c.* 40°C (Wolf *et al.* 1996, 1998; Farley 2002). However, these temperature limits are known to vary with crystal dimensions, compositional zonation, eU concentration (eU = [U] + 0.235 × [Th]) and accumulated radiation damage (Farley 2000; Reiners & Farley 2001; Shuster *et al.* 2006). Moreover, small fluctuations in these factors are magnified by extended residence in the AHePRZ, commonly resulting in dispersed AHe ages (Flowers & Kelley 2011). In zircon (U-Th)/He dating, alpha particles are partially retained between *c.* 150 and 190°C (ZHe Partial Retention Zone – ZHePRZ), and promptly expelled at temperatures higher than 190°C (Reiners et al 2018 book). Similarly to AHePRZ, the ZHePRZ is affected by compositional zonation, eU concentration, accumulated radiation damage and protracted residence at low temperatures (Reiners *et al.* 2002, 2004; Nasdala *et al.* 2004; Reiners 2005).

The (U-Th)/He analyses were conducted in the Baja Arizona Radiogenic Helium Dating Laboratory (BARHDL), at the University of Arizona, US. Both apatites and zircons were handpicked based on morphology, size and optical clarity, using a Leica MZ16 microscope. Because apatites tend to accumulate low quantity of alpha particles due the low eU concentration (eU < 50 ppm), preference was given to clear apatites with both terminations, aiming to avoid crystals that loss ^{4}He through fractures or a highly damaged crystal lattice. On the other hand, since zircon eU usually is one or two orders of magnitude higher, we picked zircons with a wide range of opacity, which ultimately reflect the amount of accumulated radiation damage, and provide a better view of the eU influence over the ZHe age. Crystals were measured and photographed with Leica Application Suite V3, to define the diffusion domain and allow the alpha-ejection age correction (Farley *et al.* 1996), which accounts for the ejection of ^{4}He in crystal rims during decay. Nb foil tubes were used to pack the crystals for helium extraction, made using long-wavelength laser heating and measured with a quadrupole mass spectrometer. Subsequently, crystals were dissolved for the U-Th measurements, performed using a high-resolution Element2 ICP-MS. Durango standards and blank samples were systematically introduced in between analysis to guarantee reliability of the measurements.

3.3 Inverse thermal modeling

The thermal history of each sample was recreated using the program QTQt 5.7, which tests time-temperature points aiming to reconstruct a thermal history that predicts and reproduces the observed thermochronometric data (Gallagher *et al.* 2009; Gallagher 2012). We opted to run models with a minimum of user-imposed constraints, to avoid a biased thermal history. To initiate our models, a large t-T box was set with time ranging from 500 ±

50 Ma and temperature from 100 ± 100°C, time corresponding to the end of the Brasiliano/Pan-African. A final constraint was set with temperature of 20 ± 10°C at the present time. The thermal history between initial and final constraints was recreated freely by QTQt 5.7, using a temperature range of 70 ± 70°C when modeling only AFT and AHe, and up to 100 ± 100°C when ZHe data were available.

Because our current understanding of the AFT system is arguably better established than the (U-Th)/He system, trial models were run only with AFT data at first, and (U-Th)/He data were included in posterior models. Several fast runs of 20,000 interactions were made initially for each sample to set appropriate parameters during inversion (see Gallagher, 2012), and to test the variability of models using different $\partial T/\partial t$ rates. Models run only with AFT data resulted in good fit between observed and predicted ages and MTL, but the inclusion of AHe data into the models led to a considerable mismatch of the AFT data. The later models predicted older AFT ages than the observed while attempting (and usually failing) to fit all AHe ages without improving the low temperature (< 60°C) thermal history. To address this conflict and maintain a good fit of our AFT data, we used a feature from QTQt 5.7 that resamples the AHe age error in order to accept a larger degree of mismatch of AHe data. On the other hand, the inclusion of ZHe data usually better constrained the cooling time from higher temperatures (> 150°C) in the models. Final models combined all thermochronometry data available for each sample, were run for 200,000 interactions or more, and used a maximum $\partial T/\partial t$ of 10°C/Ma, compatible with a cratonic region of subdued topography. This final modeling set up permitted the proposed time-temperature paths to be well defined but not tightly limited by our constraints or by the old and dispersed AHe ages (see Results and Interpretations). During modeling, for AFT we used the D_{par} values and *c*-axis projected tracks lengths (Donelick 1993; Donelick *et al.* 1999a), the AFT annealing model from

Ketcham *et al.* (2007), and the radiation damage model from Flowers *et al.* (2009) for AHe and from Guenthner *et al.* (2013) for ZHe.

4. Results of previous thermochronometry studies in Uruguay

The first thermochronometry investigation in the UYS was made by Kollenz (2015), who obtained seven AFT ages in the shield. Five AFT central ages in the PAT and TT range between 325 ± 25 and 200 ± 20 Ma, with a mean of 260 Ma, and show a tendency to increase with the distance from the coast, although the youngest age is in the middle of the PAT. The remaining two ages, around 225 Ma, were obtained in the western part of the CDT. Track lengths were obtained from four samples from PAT, TT and CDT and display a unimodal distribution, with a range between 12.2 and 10.8 μm. Inverse thermal modeling made in these four samples using HeFTy (Ketcham 2005), show general cooling from the high limit of the AFTPRZ to surface temperature between the Carboniferous and Middle Jurassic, followed by a period of reheating until Late Cretaceous, when some samples reached temperatures up to 65 °C. A final cooling back to surface temperature was observed in all models during the Cenozoic. According to Kollenz (2015) the Paleozoic to Mesozoic cooling trend is linked to a regional exhumation, possibly related to compressional stress in the SW of Gondwana (*e.g.* Gondwanic cycle) and which has been also reported further south in Argentina and north in southernmost Brazil (Borba *et al.* 2002, 2003; Oliveira *et al.* 2016; Kollenz *et al.* 2017; Machado *et al.* 2019). They suggest that the late Mesozoic reheating phase is associated to the Paraná-Etendeka LIP, which lava flows would have buried the UYS and caused an increase in the bedrock temperature.

Gomes & Almeida (2019) published AFT ages for nine locations of the UYS. Their ages present a range from 326 ± 30 to 121 ± 19 Ma (if an outlier of 38 ± 2 Ma is ignored), suggest a positive correlation with altitude and are divided by the authors into a western domain of older ages and an eastern domain of younger ages. The MTL show a unimodal distribution and range from 12.5 to 10.0 μm. Inverse thermal modeling was made in eight samples using the outdated AFTSolve (Ketcham *et al.* 2000), a software without *c*-axis projected track lengths, and a limited number of confined tracks (usually < 45), so that the resulting models should be taken carefully. In any case, they suggest a general cooling trend until the Triassic, when samples reached stability around the lower limit of the AFTPRZ (60 °C). Some of their samples in Uruguay and southernmost Brazil suggest reheating during Cretaceous. All models show a final cooling to surface temperature after the Paleogene.

Based on a dataset of AHe and ZHe ages, Hueck *et al.* (2017) suggested a distinct thermal evolution for the UYS. They obtained 33 ZHe ages from 11 locations, with average ages between 560 and 460 Ma and acquired within zircons mostly of eU < 500 ppm. ZHe ages do not show correlation with eU, crystal size, altitude or location. Their AHe ages were obtained from 27 crystals from nine locations and show considerable dispersion, with mean ages ranging from Permian to Cretaceous. No correlation was found between AHe ages and eU or crystal size, but it is suggested that samples from the southern UYS, closer to the coast, have the youngest values. From inverse thermal models made in HeFTy, the authors suggest that the UYS reached near-surface conditions by Silurian (*c.* 420 Ma), succeeded by cycles of burial (and minor reheating) and erosion, associated to Devonian and Permian Paraná Basin deposits. Their models imply a final Mesozoic exhumation of the UYS, with restricted sedimentation, and possibly related to the tectonic stress associated with Pangea breakup. According to the authors, by the end of Mesozoic the analyzed samples would have reached surface temperature, and a Cretaceous reheating is not supported.

In summary, Kollenz (2015) models based on AFT support cooling towards near-surface conditions (T < 30°C) from Carboniferous to Jurassic, followed by reheating (up to 65 °C) in the Cretaceous and a final cooling to surface temperature during Cenozoic. Gomes & Almeida (2018) AFT models suggest a major cooling phase until the Triassic, without reaching near-surface conditions and followed by stability around 60 °C or minor reheating during the late Mesozoic, until a final cooling phase starting in the Miocene. On the other hand, Hueck *et al.* (2017) (U-Th)/He models suggest cooling to near-surface conditions by the Silurian, followed by shallow reburial (with reheat below 90 °C) and exhumation cycles until Permian and a final cooling to surface temperature during Mesozoic. Despite the temporal conflict, all authors support a complex thermal history for the region, with a main Paleo- Mesozoic cooling phase to temperatures close or below 60 °C, minor reheating episodes or protracted stability at this temperature, and a final Meso- Cenozoic cooling towards surface temperature. Remarkably, their models were made using different data and user constraints, and their cooling/heating phases imply distinct thermotectonic histories for the UYS.

5. Results and interpretations

The results from each thermochronometer and from the inverse modeling are exposed in the subsections below. General interpretations are briefly commented as well, however the particularities of the results inserted in the geological context on Uruguay are explored in the Discussion section.

5.1 Apatite Fission-tracks

We obtained AFT ages from 19 samples (Table 2), all of which passed the homogeneity chi-square test ($P\chi^2 > 5\%$) and generally did not show single grain age dispersion, which means that the central ages obtained correspond to single populations. Three samples presented minor age dispersion (UY10 = 17%, UY19 = 18% and UY32 = 18%) that could indicate a mix of apatite populations, but because they passed the chi-square test and their central ages agree with neighborhood samples, we considered them as single population also (see Supplementary Material). All obtained ages are Mesozoic, ranging from

230.9 ± 18.7 Ma to 85.8 ± 8.4 Ma (Late Triassic to Late Cretaceous), with the majority situated in the Jurassic Period. In general, the younger ages are near the coast or structural lineaments, while the older ones are hinterland, in a common distribution of ages of passive margins (Gallagher & Brown 1997). When including data from previous AFT studies in the region, a positive correlation between ages and elevation or distance to the Atlantic Ocean is observed (Fig. 3). The NPT presented simultaneously one of the oldest AFT age in our set (sample UY6 with *c.* 230 Ma, located in the north on the Isla Cristalina de Rivera) and also the youngest AFT age (UY14 with *c.* 85 Ma, in the southern-central portion of the terrane). This deviation can be related to the complexity of the NPT, composed of distinct rock associations and cut by several faults and shear zones, prone to variable exhumation within the terrane. Sample UY14 for example, the youngest one, is located near a major fault, and might reflect the last stage of tectonic reactivation of this structure at the time of Campanian rhyolitic volcanism (Gaucher et al., 2016).

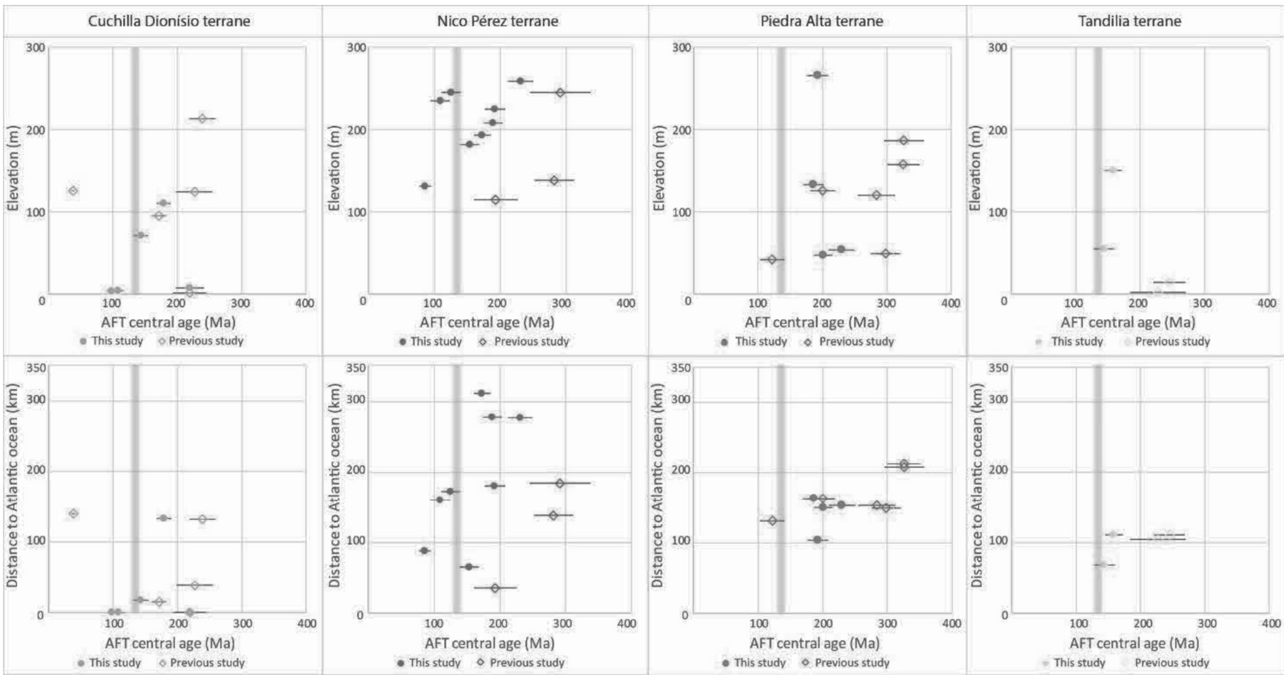

Figure 3. Compilation of AFT data available for the Uruguayan shield. Top row shows plots of AFT central ages against elevation, with a general positive correlation for the CDT, NPT and PAT. Bottom row shows AFT ages against the shortest distance to the Atlantic margin in the east, with positive correlation for the NPT and PAT as well. Vertical red bar indicates the Paraná-Etendeka LIP volcanism.

The non-projected mean track lengths (MTL) of all samples are rather medium to short, ranging from 12.7 ± 0.2 to 10.2 ± 0.2 µm (Table 2). After applying the *c*-axis projection (Donelick *et al.* 1999b), the MTL range from 13.9 to 12.3 µm, with standard deviation between 1.4 and 0.8 µm. The lengths scattering tends to be unimodal for all samples but UY29, which displays a bimodal distribution and a distinct old AFT age in SSE coastal region (CDT). In most cases, the track lengths distribution is Gaussian around the mean value or negatively skewed, with a larger proportion of longer tracks (see Supplementary Material), which can be interpreted in terms of protracted cooling (Gallagher & Brown 1999). A plot of the MTLs against AFT central ages (Fig. 4), including published data (Kollenz 2015; Gomes & Almeida 2019), does not show a clear "boomerang" shape (Green 1986), which is characteristic of reheating with partial reset of AFT ages in a region. Instead it suggests that samples went through protracted cooling without a major reheating, and with distinct parts of the shield cooling below 110 °C at different times. Measurements of the D_{par} range between 2.27 and 1.76 µm, which indicates a predominance of chlorine rich apatites, with high resistance to annealing (Carlson *et al.* 1999; Donelick *et al.* 2005).

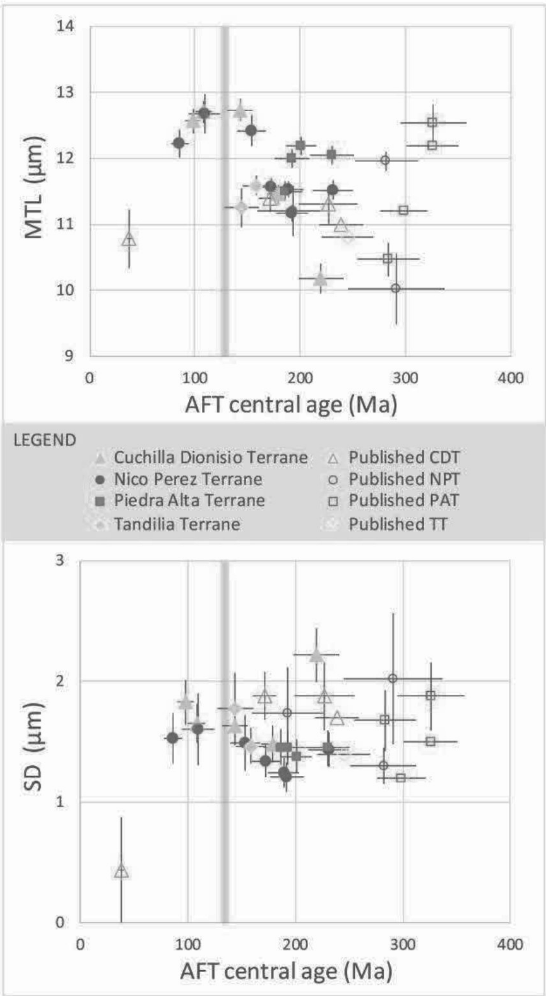

Figure 4. Compilation of AFT data available for the Uruguayan shield. In the top, AFT central ages against MTLs uncorrected for their c-axis orientation, suggesting that samples went through protracted cooling without partial resetting during the Paraná-Etendeka LIP volcanism (vertical red bar), and with distinct parts of the shield cooling below 110 °C at different times. In the bottom, plot of the AFT central ages against the standard deviation of the MTLs, which also does not show a "boomerang" shape. Error bars represent ±1σ range.

Apatite Fission Tracks analysis																		
Sample	N	ρs	Ns	ρi	Ni	ρd	Nd	Central Age	±1σ	χ2	U	Dpar	CT	MTL	±1σ	SD	*c*P. MTL	*c*P. SD
#	#	($x10^5$)	#	($x10^5$)	#	($x10^5$)	#	(Ma)	(Ma)	(%)	(ppm)	(µm)	#	(µm)	(µm)	(µm)	(µm)	(µm)
Cuchilla Dionísio Terrane																		
UY2	20	18.91	779	10.46	431	7.17	14341	179.0	10.8	88	18.5	1.87	100	11.46	0.15	1.48	13.31	0.90
UY29	20	9.16	338	4.12	152	7.17	14341	219.6	21.5	99	7.3	1.79	100	10.18	0.22	2.22	12.31	1.39
UY30	20	12.96	359	12.85	356	7.00	13999	98.1	7.4	69	23.3	2.18	100	12.57	0.18	1.83	13.89	1.43
UY31	20	15.5	369	10.76	256	7.17	14341	143.2	11.7	94	19.1	2.04	100	12.73	0.16	1.63	13.93	1.31
UY32	20	15.14	542	13.85	496	7.17	14341	108.3	8.1	11	24.5	1.91	100	12.71	0.17	1.65	14.08	1.07
Nico Pérez Terrane																		
UY1	20	19.25	460	9.92	237	7.17	14341	192.1	15.4	99	17.6	1.82	100	11.17	0.12	1.21	13.00	0.80
UY6	20	12.29	515	5.25	220	7.17	14341	230.9	18.7	95	9.3	1.88	100	11.52	0.14	1.44	13.31	0.88
UY7	20	17.97	532	9.19	272	7.00	13999	189.0	14.2	98	16.7	1.81	100	11.53	0.12	1.25	13.24	0.84
UY8	20	13.24	507	7.60	291	7.17	14341	172.7	12.8	99	13.5	1.90	100	11.56	0.13	1.34	13.30	0.83
UY10	20	4.06	204	3.17	159	7.00	13999	125.4	14.1	59	5.7	1.87	-	-	-	-	-	-
UY11	20	5.3	114	4.84	104	7.17	14341	109.2	14.8	100	8.6	1.79	30	12.68	0.29	1.61	13.87	1.23
UY14	20	3.47	191	4.05	223	7.17	14341	85.8	8.4	100	7.2	1.88	52	12.23	0.21	1.53	13.72	1.16
UY21	20	8.39	308	5.42	199	7.17	14341	153.6	14.0	94	9.6	1.87	42	12.43	0.23	1.49	13.84	1.04
Piedra Alta Terrane																		
UY16	20	10.71	422	5.38	212	7.00	13999	192.3	16.3	100	9.8	1.76	100	12.00	0.15	1.45	13.58	0.99
UY25	20	18.78	417	8.06	179	7.17	14341	229.9	20.6	82	14.3	1.99	100	12.05	0.14	1.45	13.54	1.10
UY26	20	22.09	612	10.87	301	7.17	14341	201.1	14.3	74	19.2	2.27	100	12.20	0.14	1.38	13.73	0.87
UY27	20	12.69	387	6.59	201	7.00	13999	186.1	16.2	99	12.0	2.03	100	11.50	0.15	1.46	13.18	1.04
Tadilia Terrane																		
UY18	20	13	360	7.94	220	7.00	13999	158.5	13.6	100	14.4	1.77	100	11.59	0.15	1.47	13.30	0.95
UY19	20	13.79	222	9.63	155	7.17	14341	144.0	16.2	53	17.1	1.86	38	11.25	0.29	1.78	13.08	1.11

Table 2: Apatite fission-track data from the Uruguayan shield. Ages were calculated using ζ= 280.17. N: number of grains analyzed; ρs: spontaneous track density; Ns: number of spontaneous tracks counted; ρi: induced track density; Ni: number of induced tracks counted; ρd: dosimeter tracks density; Nd: number of tracks used to determine ρd; χ2: chi-square probability of single population; U: estimated value of uranium content; Dpar: mean etch pit diameter; CT: confined tracks measured; MTL: mean track length; SD: standard deviation of mean track length distribution; cP.MTL: c-axis projected mean track length; cP. SD: standard deviation of c-axis mean track lenght; (-): data not available.

5.2 Apatite (U-Th)/He

Apatites from 14 locations were selected for AHe analysis, in total representing 42 single crystal ages (Table 3). The obtained ages present are widely dispersed, not only between samples and terranes, but also among apatites from each sample, in a similar way as observed by Hueck *et al.* (2017). The AHe uncorrected ages range throughout the Phanerozoic, but the majority of them are Mesozoic. No reduction in the age dispersion is observed after applying the Ft correction (Farley *et al.* 1996). Furthermore, the AHe ages obtained are mostly older than the AFT ages from the same location, portraying an inverse pattern that is often observed in cratonic regions (Flowers & Kelley 2011).

A common approach to investigate AHe ages dispersion is to evaluate the influence of the crystal radius and integrity (Reiners & Farley 2001; Brown *et al.* 2013), and of the effective uranium (eU) content of crystals (Flowers *et al.* 2007), factors that commonly affect AHe ages. Our samples do not show a clear correlation between ages and these parameters, suggesting that other factors are responsible for the AHe ages dispersion. Several variables can influence AHe ages, including U and Th zonation (Farley *et al.* 1996; Flowers & Kelley 2011), U-rich inclusions (Stockli *et al.* 2000), ^{4}He implantation from U-rich neighbor minerals and phases (Murray *et al.* 2014), accumulated radiation damage on the crystal lattice (Green & Duddy 2006; Shuster *et al.* 2006), among others – see Wildman *et al.* (2016) for a summary of the influence of these and others factors. These variables can be used to explain the dispersion in some samples, as in sample UY2, collected from a region of eU rich granites and that present old AHe ages and high values of ^{4}He for its eU content, making ^{4}He implantation or U-rich inclusions likely occurrences. Figure 5 shows apatites from samples UY8, UY27 and UY32 that were subjected of AFT analysis and exhibits zonation and inclusions. Although the images are not from crystals used for AHe dating, they represent common features in these samples that potentially affected our AHe ages. Considering this, we opted to report in Figure 2 the youngest AHe age for each location, which potentially represents the age least affected by factors such as implantation and inclusions. As such, these would be closer to the actual cooling age of the sample and correspond to the standard closure temperature (Dodson 1973) of the AHe system. The presence of inclusions, zonation or defects in the crystal lattice can lead to the highly dispersed ages and mask the common correlations between ages and eU or crystal radius. However, because dispersion is observed in most of our samples, a more general approach is desired to explain our results, as suggested later in the Discussion section.

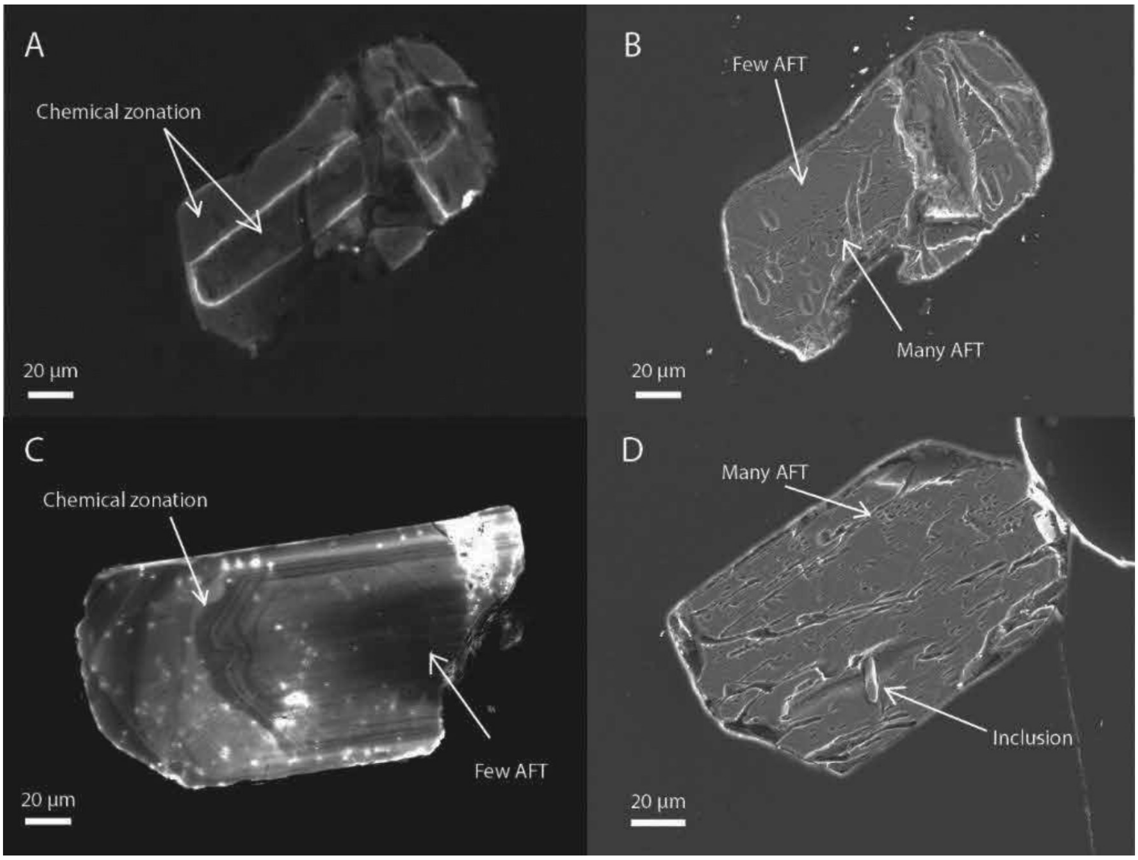

Figure 5. Photomicrographs of apatites showing factors that can affect the (U-Th/He) analysis and cause significant age inaccuracies. (A,B) Cathodoluminescence and secondary electron images from the same apatite from UY32 showing a brightly marked chemical zonation coincident with a fission-track density zonation. (C) Cathodoluminescence from apatite from UY8 showing chemical zonation and a low density of tracks in the center. (D) Secondary electron image from apatite from UY27 showing inclusion and a higher density of tracks in the rims.

Apatite (U-Th)/He analysis																			
Sample	Crystal	U	Th	Sm	He	eU	Term.	Radius	Age Unc.	±1σ	Ave. Unc.	SD	±1σ	Ft	Age Corr.	±1σ	Ave. Corr.	SD	±1σ
#	#	(ppm)	(ppm)	(ppm)	(nmol/g)	(ppm)	#	(μm)	(Ma)	(Ma)	(Ma)	(Ma)	(Ma)	#	(Ma)	(Ma)	(Ma)	(Ma)	(Ma)
Cuchilla Dionísio Terrane																			
UY2	1	59.92	130.15	488.89	146.82	92.67	1	57.38	292.10	5.96	441.09	106.69	61.60	0.74	392.38	8.07	546.46	109.62	63.29
	2	21.79	61.86	368.63	101.75	37.99	1	79.51	494.97	10.11				0.81	608.67	12.54			
	3	8.78	24.84	305.88	45.05	16.03	2	92.53	536.20	11.07				0.84	638.33	13.27			
UY30	1	8.13	12.82	214.17	7.49	12.14	2	42.71	120.51	2.68	107.98	10.71	6.18	0.67	180.31	4.03	152.31	21.71	12.53
	2	24.29	19.84	478.29	15.14	31.18	2	55.35	94.34	1.31				0.74	127.41	1.77			
	3	9.85	8.15	18.56	7.00	11.85	1	53.89	109.09	1.69				0.73	149.21	2.33			
UY32	1	59.86	11.48	467.66	38.88	64.74	2	40.45	113.17	2.51	135.58	50.08	28.91	0.66	171.81	3.83	196.36	69.34	40.03
	2	45.55	5.08	421.35	22.73	48.72	1	46.78	88.60	1.97				0.70	126.41	2.83			
	3	46.53	4.36	447.24	54.10	49.65	1	46.86	204.97	4.58				0.70	290.85	6.54			
UY24	1	3.91	2.21	271.49	4.03	5.70	1	45.94	155.03	4.61	211.19	56.16	39.71	0.71	219.65	6.55	314.97	95.32	67.40
	2	2.22	1.89	469.70	4.75	4.87	1	34.84	267.35	10.79				0.65	410.29	16.33			
Nico Pérez Terrane																			
UY1	3	14.64	2.24	157.52	8.04	15.90	1	62.41	96.34	2.15	131.16	29.66	17.13	0.77	125.01	2.80	170.41	32.60	18.82
	4	19.69	54.24	222.63	22.89	33.42	1	47.23	128.32	1.81				0.69	186.17	2.65			
	5	26.26	25.87	124.55	30.01	32.90	2	95.87	168.83	2.52				0.84	200.06	3.00			
UY6	1	7.99	36.96	66.71	15.38	16.96	2	66.62	167.83	3.39	262.62	67.12	38.75	0.77	218.10	4.42	346.05	90.48	52.24
	2	9.03	43.73	74.69	32.68	19.61	2	59.49	305.66	6.20				0.75	409.89	8.37			
	3	5.90	24.48	68.68	20.36	11.95	2	64.67	314.37	6.41				0.77	410.17	8.42			
UY8	1	4.54	15.55	44.52	7.53	8.39	1	47.93	166.91	2.27	182.64	40.46	18.09	0.69	241.31	3.32	281.44	63.42	28.36
	2	21.50	41.04	72.27	21.49	31.45	2	38.08	126.17	1.46				0.63	201.46	2.37			
	3	11.28	50.36	358.19	30.32	24.75	2	41.09	234.61	3.28				0.65	362.35	5.08			
	4	11.46	44.23	88.01	24.41	22.22	1	39.51	202.88	2.86				0.63	320.65	4.56			
UY11	1	4.25	36.85	694.43	20.01	16.14	2	52.86	265.25	3.24	208.62	48.20	27.83	0.72	367.60	4.44	285.99	61.74	35.65
	2	6.21	43.76	359.92	13.63	18.14	1	45.83	147.43	1.89				0.68	218.29	2.79			
	3	8.34	74.17	621.66	30.96	28.61	1	71.44	213.17	2.59				0.78	272.07	3.29			
UY14	1	3.10	23.24	96.80	4.47	9.00	2	73.47	94.61	1.22	103.01	16.33	7.30	0.79	120.26	1.55	133.43	20.82	9.31
	2	3.92	24.81	91.44	6.31	10.16	2	62.63	117.32	1.33				0.75	155.65	1.76			
	3	5.86	22.81	69.82	4.94	11.53	2	62.61	80.37	0.90				0.76	106.26	1.19			
	5	2.84	20.74	85.27	5.10	8.09	2	74.51	119.73	1.42				0.79	151.57	1.79			
UY21	1	18.58	52.98	716.38	15.92	97.71	1	41.89	91.78	1.90	105.94	14.16	8.18	0.68	139.63	2.90	152.94	13.31	7.69
	3	9.90	20.42	218.52	9.79	16.23	2	52.63	120.10	2.57				0.71	166.25	3.58			
Piedra Alta Terrane																			
UY16	1	6.08	24.39	164.32	14.82	12.56	2	54.18	224.94	2.63	250.26	18.01	10.40	0.73	310.02	3.64	328.44	23.04	13.30
	2	8.40	23.61	171.26	20.68	14.73	2	55.50	265.35	2.98				0.74	360.93	4.09			
	3	10.39	8.93	103.22	18.10	12.96	2	85.64	260.49	3.26				0.83	314.37	3.96			
UY25	1	56.87	38.42	271.62	64.15	67.13	1	49.97	176.95	3.78	258.83	59.84	34.55	0.72	247.45	5.32	368.18	85.42	49.32
	2	25.50	24.77	219.10	55.67	32.33	1	56.98	318.28	6.78				0.75	424.81	9.15			
	3	27.21	24.40	212.86	51.57	33.92	2	39.58	281.27	6.07				0.65	432.29	9.47			
UY27	1	13.43	16.16	314.13	30.29	18.69	2	46.35	311.03	3.97	263.80	34.10	19.69	0.70	445.54	5.76	388.25	40.51	23.39
	2	23.25	42.01	431.60	42.83	35.11	2	39.54	231.74	2.76				0.64	359.42	4.34			
	3	19.50	36.16	468.71	39.06	30.16	2	46.06	248.63	2.92				0.69	359.80	4.27			
Tandilia Terrane																			
UY18	1	9.44	2.74	129.44	12.50	10.69	2	49.67	222.16	6.50	201.68	21.16	10.58	0.72	308.79	9.10	289.96	34.86	17.43
	2	16.26	12.18	136.90	18.21	19.75	2	50.06	172.54	3.98				0.72	241.10	5.60			
	3	12.28	4.32	108.17	15.50	13.79	2	40.05	210.33	5.11				0.66	320.01	7.86			

Table 3: Summary of Apatite (U-Th)/He ages and parameters. Crystal dimensions were used to estimate an equivalent spherical radius. eU, total uranium content; Term, number of crystal terminations; Unc., uncorrected; Corr., corrected; SD, standard deviation; Ft, alpha ejection factor for age correction.

5.3 Zircon (U-Th)/He

A total of 40 zircons were dated from eight locations across the UYS (Tab. 4). Single crystal ZHe ages range through the entire Paleozoic and show a strong negative correlation with eU, unlike our AHe ages (Fig. 6). Such negative correlation is common in cratonic regions and usually is attributed to long-term accumulation of radiation damage in the crystals. Zircons with high eU and long low-temperature histories are prone to develop a damage net within the crystalline lattice, which increases the diffusivity and loss of alpha particles, thus resulting in younger ages (Reiners 2005; Guenthner *et al.* 2013). Considering this, we opted to show in the map (Fig. 2) the oldest single grain ZHe age for each location, usually Cambrian/Ordovician for the NPT and CDT samples, and Permian for the PAT. The oldest ZHe age potentially represents the cooling age of the least damaged zircon analyzed, likely closer to the beginning of the ^{4}He accumulation within the sample and to the standard closure temperature of the ZHe system. No correlation between ZHe ages and crystal radius, location or altitude was observed in our samples.

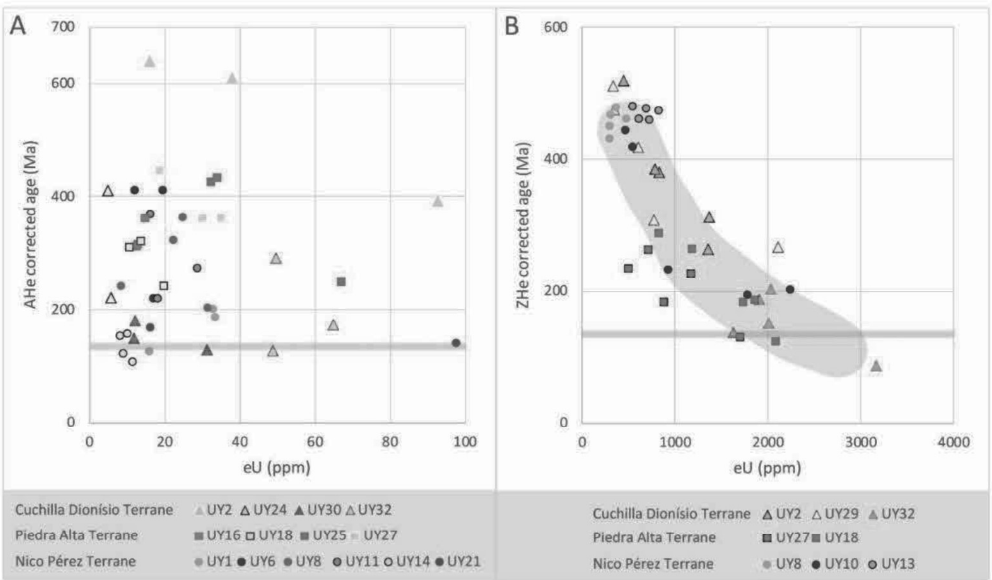

Figure 6. Plots of (U-Th/He) corrected ages against effective uranium content (eU = [U] + 0.235 × [Th]). (A) AHe ages showing variable intrasample behavior and no apparent general trend. (B) ZHe ages clustered or showing a negative correlation intrasample and as general trend. Horizontal bar indicates the Paraná-Etendeka LIP volcanism.

Zircon (U-Th)/He analysis																	
Sample	Crystal	U	Th	He	eU	Radius	Age Unc.	±1σ	Ave. Unc.	SD	±1σ	Ft	Age Corr	±1σ	Ave. Corr.	SD	±1σ
#	#	(ppm)	(ppm)	(nmol/g)	(ppm)	(μm)	(Ma)	(Ma)	(Ma)	(Ma)	(Ma)	#	(Ma)	(Ma)	(Ma)	(Ma)	(Ma)
Cuchilla Dionísio Terrane																	
UY2	1	1216.02	636.19	1592.79	1365.52	36.94	212.40	3.02	273.11	68.31	30.55	0.68	311.46	4.49	371.45	86.13	38.52
	2	773.03	215.67	1214.88	823.71	39.61	267.17	5.04				0.70	379.04	7.24			
	3	741.36	175.63	1292.37	782.64	52.87	298.24	5.68				0.77	385.10	7.41			
	4	395.44	195.09	957.90	441.28	47.41	389.04	7.28				0.75	518.30	9.84			
	7	1267.26	388.53	1480.69	1358.56	48.81	198.68	3.71				0.75	263.37	4.96			
UY29	1	543.50	270.19	1130.77	606.99	61.94	335.50	4.39	299.50	80.16	35.85	0.80	417.01	5.52	395.12	94.15	42.11
	2	293.29	213.03	693.26	343.35	50.85	362.95	4.57				0.76	475.00	6.09			
	3	1963.03	622.64	2228.84	2109.35	42.73	192.73	2.84				0.72	266.84	3.97			
	4	298.36	167.44	736.46	337.71	50.99	390.86	5.61				0.77	509.99	7.43			
	5	704.82	281.30	912.64	770.93	39.63	215.49	3.13				0.70	306.73	4.52			
UY32	1	2844.44	1344.08	1280.10	3160.30	94.20	74.66	1.03	121.47	29.46	13.18	0.87	86.22	1.20	152.75	40.98	18.33
	2	1943.91	245.54	1307.62	2001.62	59.78	119.95	1.73				0.80	150.63	2.18			
	3	1857.49	725.71	1768.94	2028.03	57.63	159.57	2.22				0.79	202.44	2.83			
	4	1138.28	3274.83	1505.60	1907.87	55.28	144.52	1.60				0.77	187.89	2.09			
	5	1542.94	344.60	960.09	1623.92	59.83	108.67	1.50				0.80	136.58	1.90			
Nico Pérez Terrane																	
UY8	1	438.83	158.79	1033.20	476.15	77.94	388.74	6.15	377.98	21.07	9.42	0.84	460.49	7.35	456.99	16.15	7.22
	2	281.82	94.67	569.75	304.06	55.21	337.27	5.32				0.78	430.51	6.87			
	3	280.84	77.47	647.22	299.04	88.50	387.67	6.27				0.86	449.53	7.32			
	4	350.88	76.05	817.60	368.75	70.52	396.72	5.74				0.83	478.21	6.98			
	5	281.90	113.49	653.05	308.57	64.82	379.52	5.32				0.81	466.22	6.61			
UY10	2	1519.54	1104.20	1203.76	1779.03	32.76	124.16	1.53	213.19	89.58	40.06	0.64	193.48	2.43	297.42	109.43	48.94
	3	1821.40	1769.65	1672.24	2237.27	37.42	137.00	1.65				0.68	201.41	2.47			
	4	758.05	703.75	812.20	923.43	39.14	160.89	1.98				0.69	231.92	2.90			
	6	415.63	219.89	836.49	467.30	43.53	322.77	5.21				0.73	443.12	7.25			
	7	489.04	235.10	969.29	544.29	52.03	321.12	5.19				0.77	417.14	6.82			
UY13	1	646.57	326.51	1441.94	723.30	54.84	358.30	6.20	365.08	12.08	5.40	0.78	458.57	8.03	469.36	8.45	3.78
	2	628.19	257.97	1467.16	688.81	60.34	381.89	6.69				0.80	476.73	8.45			
	3	491.98	235.19	1140.75	547.25	54.63	374.08	6.54				0.78	478.93	8.48			
	4	770.65	247.05	1600.27	828.70	44.30	347.24	5.86				0.73	472.45	8.09			
	5	560.25	224.84	1242.32	613.09	57.29	363.90	6.07				0.79	460.11	7.76			
Piedra Alta Terrane																	
UY27	1	851.37	116.24	755.00	878.69	90.84	157.22	2.19	170.76	40.11	17.94	0.86	182.07	2.54	206.24	46.65	20.86
	2	1102.95	316.03	1163.28	1177.22	60.71	180.43	2.46				0.80	225.73	3.10			
	3	1629.90	301.28	945.84	1700.71	60.34	102.28	1.44				0.80	128.27	1.81			
	4	483.89	69.39	525.97	500.19	68.89	191.79	3.14				0.82	233.07	3.84			
	5	670.02	204.32	876.64	718.04	80.79	222.08	3.49				0.85	262.08	4.14			
Tandilia Terrane																	
UY18	1	2012.46	328.91	1106.92	2089.76	59.72	97.46	1.61	154.81	42.01	18.79	0.80	122.52	2.03	207.89	59.07	26.42
	2	1670.14	299.44	1299.07	1740.51	47.60	136.83	1.86				0.75	182.88	2.51			
	4	1771.17	383.20	1365.69	1861.22	43.11	134.55	1.81				0.72	185.87	2.52			
	5	1105.25	334.62	1245.33	1183.88	44.39	191.87	2.58				0.73	262.18	3.56			
	6	784.68	167.61	965.85	824.07	46.85	213.35	3.77				0.75	286.00	5.10			

Table 4: Summary of Zircon (U-Th)/He ages and parameters. Crystal dimensions were used to estimate an equivalent spherical radius. eU, total uranium content; Unc., uncorrected; Corr., corrected; SD, standard deviation; Ft, alpha ejection factor for age correction.

5.4 Inverse modeling

The thermal history of 19 locations was computed by inverse modeling and the results can be divided into two main groups with distinct cooling patterns. All models use AFT data as baseline, thermochronometer with the most consistent regional results and those physical proprieties that are better understood in the scientific community, but most of the models include (U-Th)/He data as well. Final models display a good fit between observed and predicted AFT ages and MTL, a good fit of ZHe ages and usually a poor fit of AHe ages. Representative models are shown in Figure 7 and the final models of each sample can be found in the Supplementary Material.

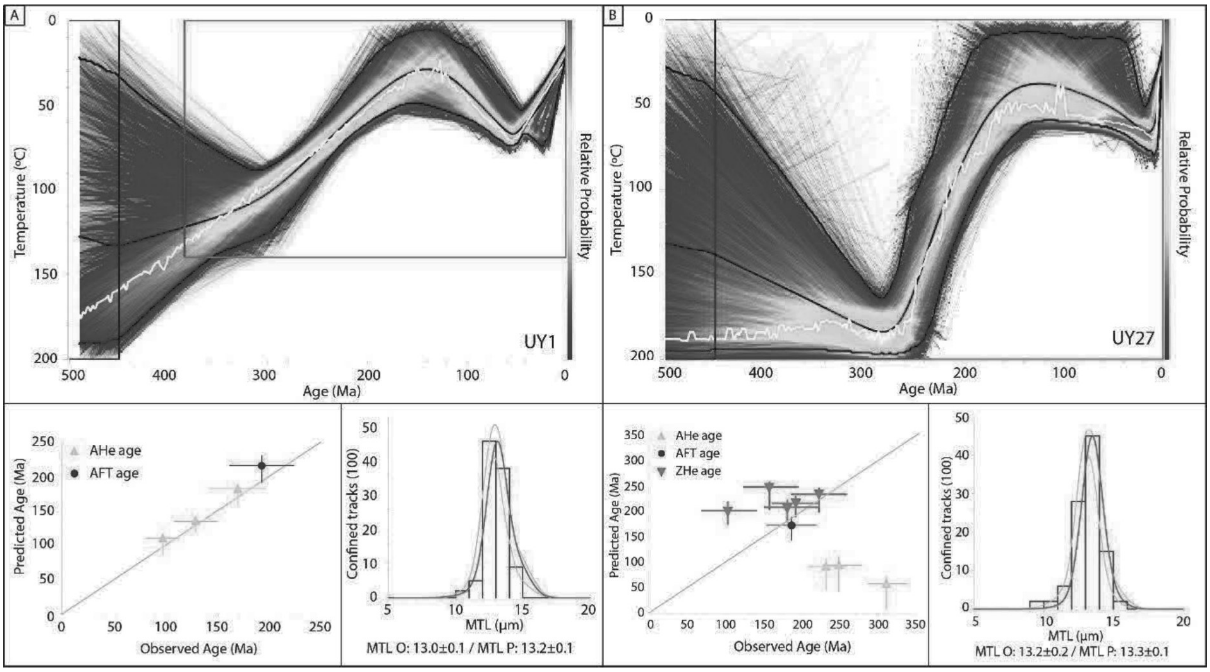

Figure 7. Panel of representative inverse thermal models from Group 1. (A) On the top: Model for sample UY1. Black line represents the mean cooling trajectory, white line the maximum mode and colored pathway the 95% confidence interval with relative probability scale. Black rectangle is the start constraint box for the model, red box the prior to test thermal paths (see Gallagher, 2012). Bottom left: fit between observed ages and predicted ages by the model, including ±1σ range. Bottom right: track length distribution with values of MTL observed and predicted by the model. (B): Same as in (A) but for sample UY27, with ZHe data.

Group 1 is composed of samples UY1, UY2, UY6, UY7, UY8, UY16, UY18, UY25, UY26 and UY27, located essentially in the west and NW of the shield (PAT, TT and northern part of the NPT). Models from these samples show passage through the AFTPRZ between *c.* 300 and 180 Ma (Fig. 8), with cooling rates varying between 0.60 and 0.32 ºC/Ma. In most cases, entrance in the AFTPRZ (*c.* 110 ºC) occurs in the Carboniferous-Permian transition, while cooling out from the zone (*c.* 60ºC) occurs by Late Jurassic-Early Jurassic. Samples UY18 and UY27, which present relatively young ZHe ages, went through the AFTPRZ slightly later and faster (*c.* 0.90 ºC/Ma) than the general trend. Models from Group 1 suggest that in Early Cretaceous all these samples might have reached surface temperatures, although it cannot be precisely constrained by our AHe data (Fig. 7). Afterwards, all models support a subtle reheating phase, that possibly lasted until the end of the Paleogene and raised temperatures slightly over 60 ºC in some samples. This reheating is at the limit of the AFT method resolution, and possibly a modeling artifact (Jonckheere 2003), a reflection of the considerably short length of the confined tracks of these samples, usually below 12 µm, which would require a prolonged time in the AFTPRZ. A final cooling towards surface temperature takes place by the Miocene. Sample UY29 resulted in a thermal history similar to Group 1 but with earlier and faster passage through the AFTPRZ, at a rate of 0.88 ºC/Ma. Cooling into the AFTPRZ occurs by the Devonian-Carboniferous transition with an exit by the Permian. The model from this sample shows stability at temperatures around 30 to 50 ºC until the Cretaceous, when a reheating phase occurred raising the temperature to 75 ºC. A final cooling towards surface conditions is observed after the Paleocene. Sample UY29 is located in the extreme SE of the shield, where most samples present thermal histories belonging to Group 2.

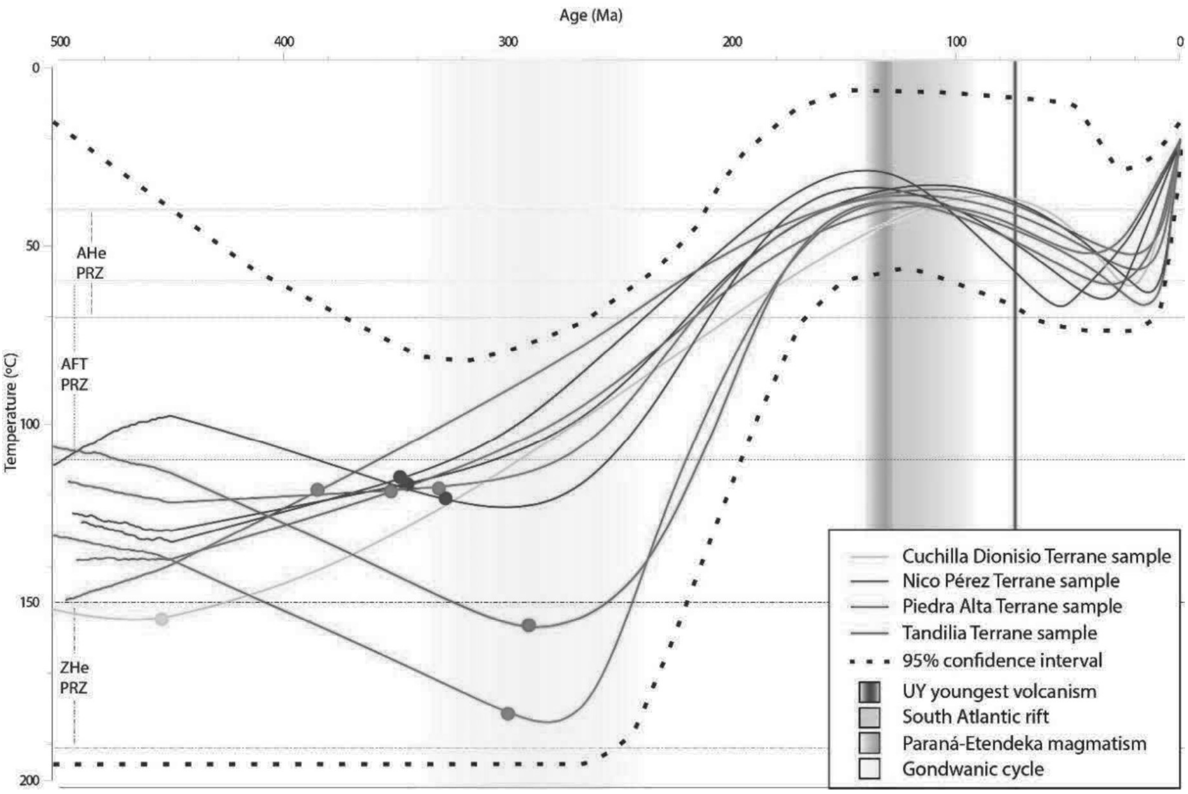

Figure 8. Mean cooling trajectories of inverse models for samples from Group 1. Dashed bold lines represent the superposition of the 95% confidence interval of individual models. Dots indicate point after which

trajectory relative probability is over 50 % inside the confidence interval. i.e. model curve before the dot is poorly constrained. Approximate interval of PRZ of each thermochronometer indicated with dashed horizontal lines. Main thermotectonic events in the region are indicated as shaded bars: Gondwanic cycle (c. 340 to 250 Ma) (Milani & De Wit, 2014), Paraná-Etendeka LIP (138 to 125 Ma) (Rossetti et al. 2014) and Atlantic Ocean opening (130 to 113 Ma) (Stica et al. 2014).

Group 2 is composed of samples UY10, UY11, UY14, UY19, UY21, UY30, UY31 and UY32. These samples are located mostly in the center and SE of the shield (NPT and CDT), and are often near shear zones. Unlike Group 1, the models for these samples lack a Late Cretaceous reheating phase, and show a monotonic cooling towards surface since early Mesozoic. The time of cooling into the AFTPRZ occurs later than Group 1 and is variable among the samples, ranging between the Permian and Jurassic. Cooling occurs at rates between 0.30 and 0.71 ºC/Ma, and during the Cretaceous all samples reached temperatures below 60 ºC. Although Group 2 corresponds to protracted and monotonic thermal histories, it should be considered that some of these samples have a limited number (< 50) of confined tracks to be used during modeling, thus their models are less robust. Nonetheless, all of them have younger AFT ages and higher track length values (MTL) than Group 1, with lengths usually above 12.2 μm, even when 100 confined tracks were measured. Therefore, their monotonic thermal histories can represent Mesozoic tectonic activity in faults/shear zones or at the margins of the shield, especially near the Atlantic Ocean, but can also reflect their long and often limited number of confined tracks, which do not require a protracted period in the AFTPRZ or a reheating phase to shorten them as in Group 1.

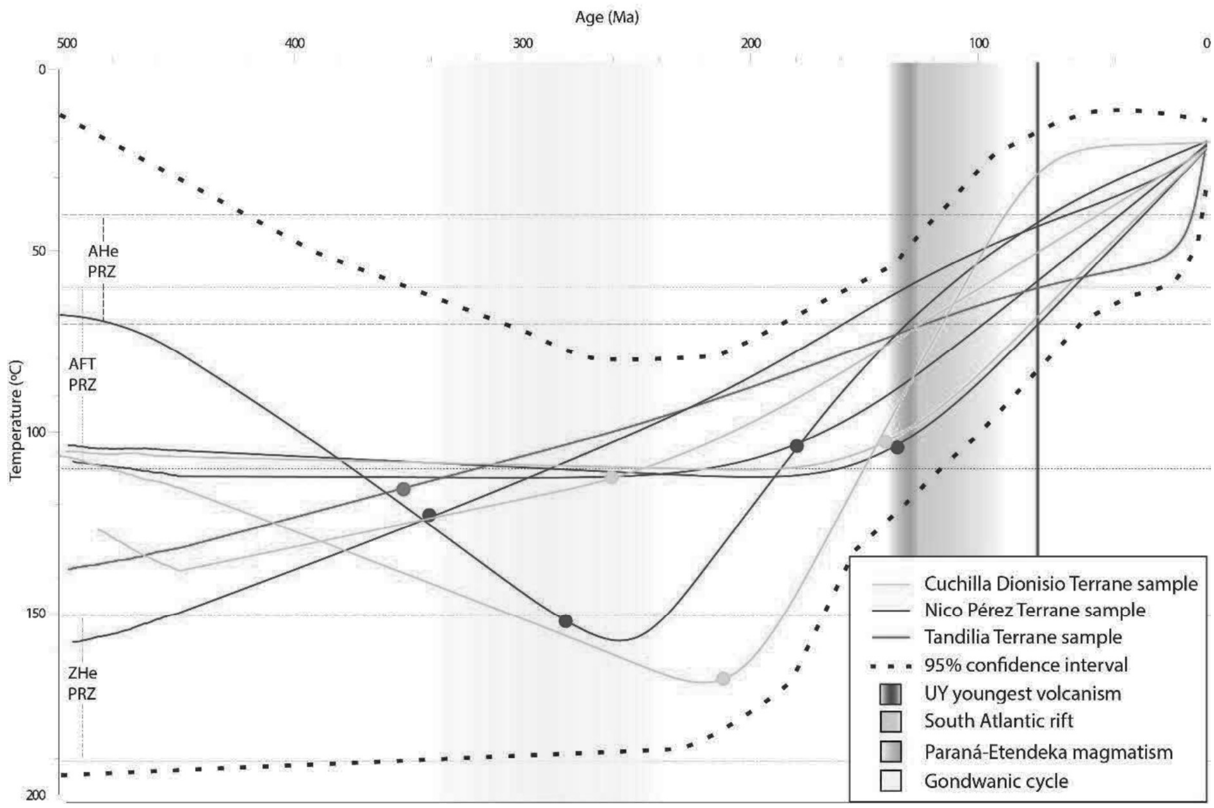

Figure 9. Mean cooling trajectories of inverse models for samples from Group 2. Dashed bold lines represent the superposition of the 95% confidence interval of individual models. Dots indicate point after which trajectory relative probability is over 50 % inside the confidence interval. i.e. model curve before the dot is poorly constrained. Approximate interval of PRZ of each thermochronometer indicated with dashed horizontal lines. Main thermotectonic events in the region are indicated as shaded bars: Gondwanic cycle (c. 340 to 250 Ma) (Milani & De Wit, 2014), Paraná-Etendeka LIP (138 to 125 Ma) (Rossetti et al. 2014) and Atlantic Ocean opening (130 to 113 Ma) (Stica et al. 2014).

6. Discussion and integration

In this study we combined three thermochronometers to investigate the cooling history of the Uruguayan shield. We presented a new dataset with 19 AFT, 42 AHe and 40 ZHe ages, plus the inverse thermal histories modeled for 19 locations. This dataset, combined with information from previous works (Kollenz 2015; Hueck *et al.* 2017; Gomes & Almeida 2019) provides an extensive coverage of the low-temperature history of the UYS. Based on the integration of these data, we characterized the thermal evolution of the shield during the Phanerozoic and discuss the exhumation of the basement, taking into account the apparent disparities between previous models.

6.1 Thermochronometry ages

All AFT ages obtained in this work are much younger than the host rock stratigraphic age and the last orogenic cycle that affected the region (Gondwana assembly during the Brasiliano/Pan-African cycle, late Neoproterozoic-Cambrian). Thus, we interpret our AFT ages as cooling ages that represent exhumation of the basement due to denudational events. There is good agreement between our AFT ages and those obtained by Kollenz (2015) and Gomes & Almeida (2018), totaling a combined dataset of 36 AFT ages across the UYS. Although the shield does not have significant topographic variations, a plot of the AFT central ages against sample elevation, including the works aforementioned, presents clear positive correlations for the CDT, NPT and PAT (Fig. 3). Ages also tend to increase with the distance from the South Atlantic Ocean, a common pattern observed in continental passive margins (Gallagher & Brown 1997). The PAT, representative of the Rio de La Plata Craton, and the northern part of the NPT, arguably part of the craton as well, concentrates the older AFT ages in Uruguay. Remarkable is the similarity between the confined track lengths in the three works, both in values and distributions, which reveal MTL of short to medium values, independently of the location in the shield. This pattern of tracks with reduced lengths implies that the samples went through a long period at temperatures close or inside the AFTPRZ, allowing continuous annealing of the tracks. The medium-high D_{par} values of our samples, indicative of fairly high resistance to annealing (Carlson *et al.* 1999; Donelick *et al.* 2005), reinforce this interpretation.

Regarding the (U-Th/He) data, our AHe ages tend to be slightly older and present higher dispersion when compared to those obtained by Hueck *et al.* (2017), who reported mainly Permian to mid-Cretaceous ages, but discarded several older crystals. Although the AHe represents a lower temperature thermochronometer than the AFT system, our AHe ages are usually older than AFT ages from the same sample, in an inverse pattern common in cratonic regions (Flowers & Kelley 2011). This inverted behavior is characteristic for apatites with eU > 15 ppm subject to prolonged residence at temperatures below 70 °C, and augmented by reheating episodes that do not reset the AHe ages (Shuster *et al.* 2006; Reiners *et al.* 2018). The wide dispersion of AHe ages within a sample can be attributed to internal factors, such as chemical zonation and alpha implantation, among others, that affect single aliquots. However, because inversion of AHe and AFT ages is a pattern in our dataset, and considerable dispersion of AHe ages is observed in almost every sample, this behavior must be attributed to a more embracing mechanism. Considering that our samples are of Precambrian rocks, and that our models and AFT data indicate residence at low temperatures (<110 °C) since the middle Mesozoic, it is likely that the analyzed apatites have accumulated a relatively high degree of radiation in the last 200 Ma. The damaged crystal lattice affects the diffusivity of the alpha particles within the apatites, initially increasing the retentivity of He, and resulting in abnormally old ages for the AHe system (Green & Duddy 2006; Shuster *et al.* 2006). Furthermore, Shuster *et al.* (2006) claims that apatite with variable eU content and subject to a reheating episode after significant accumulation of radiation damage might present a large span of AHe ages, being most extreme when the reheating increase temperatures close to 60 °C. Therefore, it is likely that some of our AHe ages are affected by intrasample factors, but it is plausible that the general behavior observed in the UYS is a consequence of accumulation of radiation damage in the apatites since the early Mesozoic, with dispersion augmented by an episode of subtle reheat in the region.

The accumulation of radiation damage plays a major role in our ZHe ages as well. If the density of damage sites overcome a threshold, they can become interconnected and decrease the retentivity of He, resulting in young ages owing to rapid He escape. Because a zircon's eU is usually one or two orders of magnitude higher than an apatite's eU, the connection between radioactive defects within the crystal lattice after long-term residence at shallow temperatures is very likely. Therefore, although our ZHe ages tend to be younger than the ones obtained by Hueck *et al.* (2017), this can be attributed to the difference in the eU of the zircons analyzed in each work. While we found that our dispersed ages have a clear negative correlation with eU, which varies between 299 and 3160 ppm (Fig. 6), Hueck *et al.* (2017) presented mostly zircons with eU below 500 ppm and whose ZHe ages clustered in the Cambrian. Our low eU samples present very similar ages to those from their work, indicating that most of the UYS reached temperatures within the ZHePRZ in the early Paleozoic. Additionally, the age dispersion observed by us indicates that samples passed through a protracted period of low temperatures (< 150 °C), favoring the accumulation of radiation damage that when interconnected became escape paths for the alpha particles generated within the zircons (Shuster *et al.* 2006; Reiners *et al.* 2018).

The evaluation of the thermochronometry ages alone, obtained from the three thermochronometers used in this work and integrated with ages previously published, gives important insights into the thermal behavior of the Uruguayan shield. The higher temperature thermochronometer ZHe ages suggest that most of the shield rocks currently exposed were at temperatures below 200 °C since the early Paleozoic. The AFT data, of intermediate temperature, indicate that samples passed through temperatures between 100 and 60 °C from the late Paleozoic to the middle Mesozoic. Finally, the lower temperature thermochronometer AHe suggests that our samples have been accumulating considerable amounts of radiation damage since the late Paleozoic, and that magmatic events in the region, such as the Paraná-Etendeka LIP and the South Atlantic rift, did not raise basement temperatures to the point of resetting AHe ages (> 70 °C). Nonetheless, AHe ages dispersion and inverse modeling of the thermal history of our samples suggest that these plate-wide events might have increased UYS temperature during Late Cretaceous, as discussed below.

6.2 Thermotectonic evolution of Uruguay

Previous thermotectonic models proposed for the UYS all infer a complex thermal history for the now exposed basement rocks, but are not consistent regarding the timing of cooling/reheating phases and exhumation/burial events. Based on ZHe and AHe data, Hueck *et al.* (2017) argued that the shield reached near-surface conditions (< 60 ºC) in the Silurian and went through subsidence and exhumation cycles during the Paleozoic, related to deposition of Devonian and Permian Paraná Basin sequences over the UYS. According to the authors, these depositional cycles of shallow burial and erosion did not increase basement temperatures over 90 ºC. However, models based on AFT data by Kollenz (2015) and Gomes & Almeida (2019), as well as the multi-thermochronometers models presented here, suggest that most of the shield cooled from the high end of the AFTPRZ (110 ºC) only after the Devonian. Therefore, if the UYS rocks were exposed to near surface conditions during the Silurian, a reheating to temperatures above the 110 ºC is necessary to reset the AFT thermochronometer during the Devonian.

Deposits of the Durazno Group, part of the Devonian Paraná Supersequence, are exposed in the shield NNE and overlie the eastern PAT and western NPT. Provenance studies by Uriz *et al.* (2016) support the CDT as the main source for the Durazno Group sediments, which corroborates the early onset of cooling and exhumation observed in our models for CDT samples UY2 and UY29. These models, which include ZHe, suggest temperatures above 150 ºC during the Silurian, followed by continuous cooling and exhumation of the samples towards the surface. Thus, the exposure of the CDT to near surface conditions during the Silurian followed by reburial to reset the AFT thermochronometer seems unlikely. The Durazno Group would have been deposited on a rather narrow and N-S oriented depression over the PAT and NPT terranes, which also acted as secondary and proximal detrital sources. In our models, the onset of cooling for these terranes occurs only around the Devonian-

Carboniferous boundary, so they could have been exposed to near surface conditions during the Silurian and buried by the Durazno Group to temperatures over 100 ºC to reset their AFT ages during the Devonian. However, our models for these terranes favor a simpler cooling history, fitting Mesozoic AFT ages with ZHe ages as old as Ordovician in the NPT or young as Permian in the PAT, without the need of exposure to the surface during the Silurian and burial in the Devonian. Moreover, palynomorphs and organic matter in the Durazno Group show little thermal overprint, mostly below 60 °C. All things considered and adopting an Occam's razor principle, exposure of our samples to near surface conditions in the Silurian followed by reset of AFT ages in Devonian seems unlikely, and a continuous protracted cooling of the shield since early to middle Paleozoic until the Mesozoic provide a satisfactory fit to the available data, with onset of cooling occurring earlier in the CDT than in the NPT and PAT.

The main cooling phase that led most of the shield rocks to near surface conditions seems to have started during the Carboniferous-Permian transition (Fig. 10). This denudation-induced cooling is characteristic of models from Group 1 (Fig. 8), in which most samples pass through the AFTPRZ (between 110 and 60 ºC) from *c.* 300 Ma until the Jurassic. This behavior is consistent over the PAT, TT and NPT, but less constrained on the CDT, where samples went through cooling since early Paleozoic (UY2 and UY29) or later in the Mesozoic (UY30, UY31 and UY32). Continuous cooling from late Paleozoic to middle Mesozoic is also dominant in AFT models from Kollenz (2015) and Gomes & Almeida (2019), although some samples from the latter suggest subtle reheating in this period. The onset of this cooling phase is correlated to the Gondwanic cycle, characterized by subduction of the Panthalassa Ocean and accretion of exotic terranes on the SW margin of Gondwana (Fig 1) (Scotese *et al.* 1999; Milani & Wit 2008). Intraplate stress transmission linked to these collisions reactivated basement structures below the Paraná Basin and surrounding areas (Milani & Wit 2008), with deformation and exhumation inferred from NE Argentina to southern Brazil until the Triassic (Zambrano & Urien 1970; Zerfass *et al.* 2004; Pankhurst *et al.* 2006; Oliveira *et al.* 2016; Machado *et al.* 2019). Therefore, the onset of this major cooling phase in the UYS is likely related to far field propagation stress and deformation caused by the Gondwanic cycle. Furthermore, during the Permian the Gondwana I Supersequence was deposited in the Paraná Basin, with its thickness increasing towards NW Uruguay (de Santa Ana *et al.* 2006). Paleocurrents of the lower part of this supersequence are preferentially towards the west and NW, and the alluvial, coarse syn-orogenic deposits from the upper part suggest that the Uruguayan shield was a basement high and possibly a limit for deposition (de Santa Ana 2004). However, restricted sedimentation and burial of parts of the UYS might have occurred as well, and could explain local reheating observed in some models from Gomes & Almeida (2019).

This main cooling phase of the UYS seems to have persisted until the Late Jurassic, when models suggest that our samples reached near surface temperatures (< 60 ºC). In NW Uruguay, fluvial and aeolian sandstones from the Gondwana III Supersequence (Sprechmann *et al.* 1981) indicate exposed areas of the Rio de la Plata Craton during the Early Cretaceous (Bossi *et al.* 1998; de Santa Ana 2004). The continuous and protracted cooling of the UYS, the beginning of which is likely related to intraplate deformation caused by the Gondwanic cycle, might have continued by uplift of the lithosphere preceding the South Atlantic opening (Early Cretaceous). During the Mesozoic the Brazilian margin went through broad epeirogenic uplift, proposed to be related to lithosphere thinning before Gondwana breakup (Tello Saenz *et al.* 2003; Zalán 2004; Carneiro *et al.* 2012). Cooling contemporaneous to that found in the UYS was observed in southernmost Brazil (Oliveira *et al.* 2016; Machado *et al.* 2019) and can be attributed to increased buoyancy of the lithosphere before rifting, possibly caused by the accumulation of melt in the asthenosphere underneath (Quirk & Rüpke 2018).

Remarkably, in the Early Cretaceous the voluminous extrusive magmatism of the Paraná-Etendeka Large Igneous Province covered most of the Paraná Basin, with lava flows extending from NE Argentina to central Brazil and Paraguay, and correlative units in southern Africa (Zambrano & Urien 1970; Turner *et al.* 1994; Gibson *et al.* 2006). This magmatism is often associated with the presence of the Tristão da Cunha mantle plume under the region and had its peak at *c.* 133 Ma, closely preceding the opening of the South Atlantic Ocean (Turner *et al.* 1994; Meisling *et al.* 2001; Gibson *et al.* 2006; Rossetti *et al.* 2014).

Rifting in the Atlantic Ocean propagated from SW to NE, and is characterized by intense volcanic activity around the UYS. Besides the Paraná-Etendeka LIP magmatism that covered northern Uruguay, the eastern Uruguayan continental margin possesses broad wedges of magmatic seaward-dipping reflectors, which thicknesses might reach more than a dozen kilometers and width up to one hundred (Soto *et al.* 2011; Morales *et al.* 2017; Reuber *et al.* 2019). Moreover, the spreading rates between South America and Africa increased continuously from 20 mm/yr at *c.* 125 Ma to a peak of 77 mm/yr at *c.* 80 Ma (Granot & Dyment 2015; Brune *et al.* 2016), implying in intense magmatic activity at the east of Uruguay. Furthermore, the tectonic stresses related to rifting are thought to have provoked the development of the SaLAM basins, a SW-NE oriented corridor within the shield considered to be an aborted rift precursor to the South Atlantic opening (Rossello *et al.* 2007). The Laguna Merín Basin, NE sector of the SaLAM, is filled with igneous rocks dated between 134 and 127 Ma (Cernuschi *et al.* 2015). Therefore, during the Cretaceous, the shield was surrounded by active magmatism and likely lying above the Tristão da Cunha plume influence area. It is plausible that this magmatic context had a thermal effect on the UYS, probably increasing the regional geothermal gradient, and possibly causing partial and shallow burial of the shield by lava flows (Kollenz 2015). A reheating episode starting around 140 Ma is suggested by our models from Group 1, with temperatures increasing from surface conditions to about 60 ºC during Paleogene. It has been argued that such a reheating phase is a modeling artifact caused by problems related to annealing of fission tracks on temperatures below 60 ºC on geological timescales (Jonckheere 2003), and because it is at the limit of resolution of the AFT system, thus poorly constrained. However, the coincidence in time between the beginning of this reheating phase suggested by the models and the magmatic events surrounding the UYS is notable. Moreover, our set of disperse and old AHe ages argue in favor of a slight reheat to temperatures < 70 ºC (Shuster *et al.* 2006). Therefore, the subtle reheating of the UYS during the Late Cretaceous suggested by the inverse models is supported by evidence of contemporaneous magmatism in the vicinity of the shield. The duration and magnitude of such reheating cannot be constrained by our data, but the models suggest there was regional cooling Neogene.

Finally, although our models from Group 2 are in general less robust than Group 1 due to the limited number of confined fission tracks, they concur with cooling to temperatures below 60 ºC in the Late Cretaceous, possibly reflecting tectonic adjustments during the final stages of the South Atlantic Oceanic opening, including acid volcanism dated at 77 ± 1 Ma in the southern NPT (Gaucher et al., 2016). Samples from Group 2 are located in the eastern margin of the shield or near ancient faults and shear zones, structures that played an important role during the rifting along the South American coast (Angelo *et al.* 2018). K-Ar ages on fault gouge also revealed tectonic activity in the Sierra Ballena Shear Zone during Late Cretaceous, related to breakup (Hueck *et al.* 2017). Therefore, the Gondwana breakup represents a period of intense transformations on the UYS, with movement across old basement structures, intense magmatic events surrounding the shield, and possibly a subtle reheating of the region during the Late Cretaceous. Unfortunately, the precise timing of such reheating and of the final cooling to surface temperature cannot be well defined by our AHe data, but it likely occurred during the Cenozoic.

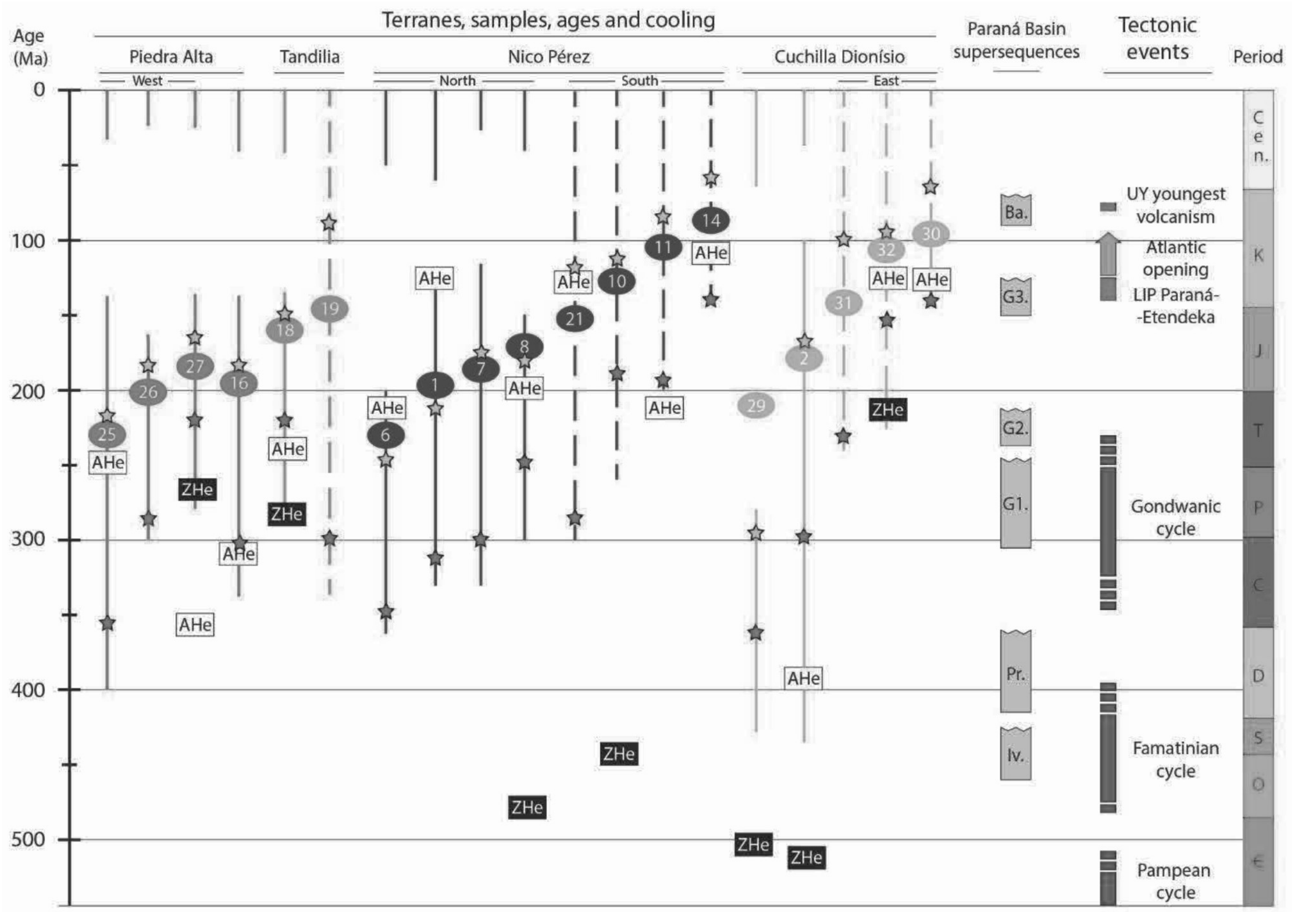

Figure 10. Chronological chart of cooling phases in the Uruguayan shield observed in inverse thermal models. Solid lines represent cooling of samples from Group 1, dashed lines from Group 2. Sample ID placed according to its AFT central age, while the oldest ZHe and youngest AHe corrected ages are reported when available. Red and blue stars indicate the approximated time of passage through temperatures of 110 and 60 ºC, respectively. Boxes on the right represent, tectonic and magmatic regional events in the vicinity of the UYS, and the sedimentary record of the Paraná Basin (supergroups Rio Ivaí - Iv., Paraná - Pr., Gondwana I - G1, Gondwana II - G2, Gondwana III - G3, and Bauru - Ba).

7. Conclusion

In this work we analyzed the thermal behavior of the Uruguayan shield based on information derived from apatite fission-tracks and apatite and zircon (U-Th)/He thermochronometry. We provided an integrated view of the thermotectonic evolution of the shield, combining 19 new AFT ages, 42 new AHe and 40 new ZHe single crystal ages with data from previous thermochronometry studies. We modeled thermal histories for 19 locations across the UYS and compared the results with previously proposed models. Our main conclusions can be summarized as follows:

1) Most of the shield reached temperatures below 200 ºC in the early Paleozoic;

2) Denudation-induced cooling was first observed in samples from the Cuchilla Dionísio Terrane, which provided a major sedimentary source for the Devonian deposits of the Paraná Basin;

3) The main cooling event of the Uruguayan shield began around the Carboniferous-Permian boundary, cooling our samples from temperatures above 100 ºC to near surface conditions (< 60 ºC) by the Jurassic;

4) The onset of this cooling phase is likely related to far field propagation of tectonic stress associated with the Gondwanic cycle on the SW margin of Gondwana;

5) Lithospheric uplift linked to South Atlantic rifting contributed to the continuity of this cooling phase until the Mesozoic;

6) The magmatic events related to Atlantic Ocean opening likely had a positive thermal effect on the Uruguayan shield, subtly increasing temperatures of the basement rocks during the Late Cretaceous; and

7) Final cooling to surface temperatures occurred in the Cenozoic, but the rates and timing cannot be precisely constrained by the available thermochronometry data.

8. Acknowledgments

The authors gratefully acknowledge the support from Shell Brasil through the “BG05: UoA-UFRGS-SWB Sedimentary Systems” project at UFRGS and the strategic importance of the support given by ANP through the R&D levy regulation. The first author thanks the CNPq scholarship (SWE 204254/2017-5) during the exchange period at the University of Aberdeen. A.R. Jelinek also thanks the support from CNPq (Project 303184/2017-5). We thank Peter W. Reiners and his team at the Baja Arizona Radiogenic Helium Dating Laboratory (US) for the (U-Th)/He analyses and support during the data evaluation.

9. References

Angelo, M., Basei, S., Frimmel, H.E., Campos, C., Eduardo, C. & Araujo, G. De. 2018. *Geology of Southwest Gondwana*. Springer International Publishing, https://doi.org/10.1007/978-3-319-68920-3.

Basei, M.A.S., Frimmel, H.E., Nutman, A.P., Preciozzi, F. & Jacob, J. 2005. A connection between the Neoproterozoic Dom Feliciano (Brazil/Uruguay) and Gariep (Namibia/South Africa) orogenic belts - Evidence from a reconnaissance provenance study. *Precambrian Research*, **139**, 195–221, https://doi.org/10.1016/j.precamres.2005.06.005.

Basei, M.A.S., Peel, E., Sánchez Bettucci, L., Preciozzi, F., Nutman, A.P., 2011. The basement of the Punta del Este Terrane (Uruguay): an African Mesoproterozoic fragment at the eastern border of the South American Río de la Plata Craton. International Journal of Earth Sciences 100, 289-304.

Beri, Á., Gutiérrez, P. & Balarino, L. 2011. Palynostratigraphy of the late palaeozoic of Uruguay, paraná basin. *Review of Palaeobotany and Palynology*, **167**, 16–29, https://doi.org/10.1016/j.revpalbo.2011.05.004.

Blanco, G., Rajesh, H.M., Gaucher, C., Germs, G.J.B. & Chemale, F. 2009. Provenance of the Arroyo del Soldado Group (Ediacaran to Cambrian, Uruguay): Implications for the paleogeographic evolution of southwestern Gondwana. *Precambrian Research*, **171**, 57–73, https://doi.org/10.1016/j.precamres.2009.03.003.

Borba, A.W. de, Vignol-Lelarge, M.L.M. & Mizusaki, A.M.P. 2002. Uplift and denudation of the Caçapava do Sul granitoids (southern Brazil) during Late Paleozoic and Mesozoic: constraints from apatite fission-track data. *Journal of South American Earth Sciences*, **15**, 683–692, https://doi.org/10.1016/S0895-9811(02)00086-X.

Borba, A.W. de, Lima, E.F. De, Vignol-Lelarge, M.L.M., Mizusaki, A.M.P., Sparrenberg, I.

& Barros, C.E. de. 2003. Significance of Late Paleozoic Fission-track Ages in Volcanic Rocks from the Lavras Do Sul Region, Southernmost Brazil. *Gondwana Research*, **6**, 79–88, https://doi.org/10.1016/S1342-937X(05)70645-6.

Bossi, J., Campal, N., 1992. Magmatismo y tectónica transcurrente durante el Paleozoico Inferior en Uruguay. In: Gutierrez- Marco, J. G., Saavedra, J., Rabano, I. (Eds.): Paleozoico Inferior de Iberoamérica. Mérida, pp 343- 356.

Bossi, J., Ferrando, L., Montaña, J., Campal, N., Morales, H., Gancio, F., Schipilov, A., Piñeyro, D., Sprechmann, P., 1998. Carta geológica del Uruguay. Escala 1:500.000. Geoeditores, Montevideo.

Bossi, J. & Cingolani, C. 2009. Extension and General Evolution of the Río de la Plata Craton. *Developments in Precambrian Geology*, https://doi.org/10.1016/S0166-2635(09)01604-1.

Bossi, J. & Gaucher, C. 2004. The cuchilla dionisio terrane, Uruguay: An allochthonous block accreted in the Cambrian to SW-Gondwana. *Gondwana Research*, **7**, 661–674, https://doi.org/10.1016/S1342-937X(05)71054-6.

Bossi, J. & Gaucher, C. 2014a. Estratigrafia del Predevonico del Uruguay. *In*: Bossi, J. & Gaucher, C. (eds) *Geología Del Uruguay - Tomo 1: Predevónico*. Montevideo, 19–42.

Bossi, J. & Gaucher, C. 2014b. Formacion Valentines. *In*: Bossi, J. & Gaucher, C. (eds) *Geología Del Uruguay - Tomo 1: Predevónico*. 171–189.

Bossi, J. & Piñeyro, D. 2014. Terreno Piedra Alta. *In*: Bossi, J. & Gaucher, C. (eds) *Geología Del Uruguay - Tomo 1: Predevónico*. Montevideo, 43–86.

Bossi, J., Ferrando, L., et al. 1998. Carta geológica del Uruguay. Escala 1:500.000.

Bossi, J., Gaucher, C., Chiglino, L., Navarro, R. & Piñeyro, D. 2014. Escama Tectonica Carape. *In*: Bossi, J. & Gaucher, C. (eds) *Geología Del Uruguay - Tomo 1: Predevónico*. 265–282.

Brown, R.W., Beucher, R., Roper, S., Persano, C., Stuart, F. & Fitzgerald, P. 2013. Natural age dispersion arising from the analysis of broken crystals. Part I: Theoretical basis and implications for the apatite (U–Th)/He thermochronometer. *Geochimica et Cosmochimica Acta*, **122**, 478–497, https://doi.org/10.1016/j.gca.2013.05.041.

Brune, S., Williams, S.E., Butterworth, N.P. & Müller, R.D. 2016. Abrupt plate accelerations shape rifted continental margins. *Nature*, **536**, 201–204, https://doi.org/10.1038/nature18319.

Carlson, W.D., Donelick, R.A. & Ketcham, R.A. 1999. Variability of apatite fission-track annealing kinetics: I. Experimental results. *American Mineralogist*, **84**, 1213–1223, https://doi.org/10.2138/am-1999-0901.

Carneiro, C.D.R., Almeida, F.F.M. de, Hasui, Y., Zalán, P. V. & Teixeira, J.B.G. 2012. Estagios Evolutivos do Brasil no Fanerozoico. *In*: Hasui, Y., Carneiro, C. D. R., Almeida, F. F. M. de & Bartorelli, A. (eds) *Geologia Do Brasil*. São Paulo, Editora Beca, 131–137.

Cernuschi, F., Dilles, J.H., Kent, A.J.R., Schroer, G., Raab, A.K., Conti, B. & Muzio, R. 2015. Geology, geochemistry and geochronology of the Cretaceous Lascano East intrusive complex and magmatic evolution of the Laguna Merín basin, Uruguay. *Gondwana Research*, **28**, 837–857, https://doi.org/10.1016/j.gr.2014.07.007.

Chiglino, L., Gaucher, C., Sial, A.N., Bossi, J., Ferreira, V.P., Pimentel, M.M., 2010. Chemostratigraphy of Mesoproterozoic and Neoproterozoic carbonates of the Nico Pérez Terrane, Río de la Plata Craton, Uruguay. Precambrian Research 182, 313-336.

Cogné, N., Gallagher, K. & Cobbold, P.R. 2011. Post-rift reactivation of the onshore margin of southeast Brazil: Evidence from apatite (U-Th)/He and fission-track data. *Earth and Planetary Science Letters*, **309**, 118–130, https://doi.org/10.1016/j.epsl.2011.06.025.

Cogné, N., Gallagher, K., Cobbold, P.R., Riccomini, C. & Gautheron, C. 2012. Post-breakup tectonics in southeast Brazil from thermochronological data and combined inverse-forward thermal history modeling. *Journal of Geophysical Research B: Solid Earth*, **117**, 1–16, https://doi.org/10.1029/2012JB009340.

De Santa Ana, H., Veroslavsky, G., Fúlfaro, V., Rossello, E. 2006. Cuenca Norte: evolución tectónica y sedimentaria del Carbonífero-Pérmico. En: Veroslavsky, G., Ubilla, M., Martínez, S. (Eds.): Cuencas sedimentarias de Uruguay. Paleozoico. Facultad de Ciencias, Montevideo, pp. 209-244.

de Santa Ana, H. 2004. *Análise Tectono-Estratigráfica Das Seqüências Chacoparanense Uruguaia (“Cuenca Norte ”)*. Universidade Estadual Paulista.

Dodson, M.H. 1973. Closure temperature in cooling geochronological and petrological systems. *Contributions to Mineralogy and Petrology*, **40**, 259–274, https://doi.org/10.1007/BF00373790.

Donelick, R.A. 1993. Method of Fission Track Analysis Utilizing Bulk Chemical Etching of Apatite. 35.

Donelick, R.A., Ketcham, R.A. & Carlson, W.D. 1999a. Variability of apatite fission-track annealing kinetics: II. Crystallographic orientation effects. *American Mineralogist*, **84**, 1224–1234, https://doi.org/10.2138/am-1999-0902.

Donelick, R.A., Ketcham, R.A. & Carlson, W.D. 1999b. Variability of apatite fission-track annealing kinetics: II. Crystallographic orientation effects. *American Mineralogist*, **84**, 1224–1234, https://doi.org/10.2138/am-1999-0901.

Donelick, R.A., O’Sullivan, P.B. & Ketcham, R.A. 2005. Apatite Fission-Track Analysis. *In*: Reiners, P. W. & Ehlers, T. A. (eds) *Low-Temperature Thermochronology: Techniques, Interpretations, and Applications*. Mineralogical Society of America, 49–94.

Faraone, M., 2018. Geología, petrografía y aspectos estructurales del extremo sur-occidental de la Zona de Cizalla Sarandí del Yí (área SW de Solís de Mataojo). Degree Thesis, Facultad de Ciencias, Montevideo.

Farley, K.A. 2000. Helium diffusion from apatite: General behavior as illustrated by Durango fluorapatite. *Journal of Geophysical Research: Solid Earth*, **105**, 2903–2914, https://doi.org/10.1029/1999JB900348.

Farley, K.A. 2002. (U-Th)/He Dating: Techniques, Calibrations, and Applications. *Reviews in Mineralogy and Geochemistry*, **47**, 819–844, https://doi.org/10.2138/rmg.2002.47.18.

Farley, K.A., Wolf, R.A. & Silver, L.T. 1996. The effects of long alpha-stopping distances on (U-Th)/He ages. *Geochimica et Cosmochimica Acta*, **60**, 4223–4229, https://doi.org/10.1016/S0016-7037(96)00193-7.

Fernandes, L.A.D.A. & Koester, E. 1999. The Neoproterozoic Dorsal de Cangucu strike-slip shear zone: Its nature and role in the tectonic evolution of southern Brazil. *Journal of African Earth Sciences*, **29**, 3–24, https://doi.org/10.1016/S0899-5362(99)00076-7.

Fernandes, L.A.D.A., TOMMASI, A., VAUCHEZ, A., PORCHER, C.C., MENEGAT, R. & KOESTER, E. 1993. Zona De Cisalhamento Transcorrente Dorsal De Canguçu: Caracterização E Importância Na Compartimentação Tectônica Do Cinturão Dom Feliciano. *Revista Brasileira de Geociências*, **23**, 224–233, https://doi.org/10.25249/0375-7536.1993233224233.

Fernandes, L.A.D.A., MENEGAT, R., et al. 1995. EVOLUÇÃO TECTÔNICA DO CINTURÃO DOM FELICIANO NO ESCUDO SUL-RIO-GRANDENSE: PARTE L - UMA CONTRIBUIÇÃO A PARTIR DO REGISTRO GEOLÓGICO. *Revista Brasileira de Geociências*, **25**, 351–374, https://doi.org/10.25249/0375-7536.1995351374.

Fleischer, R.L., Price, P.B. & Walker, R.M. 1975. *Nuclear Tracks in Solids: Principles and Applications*. California, University of California Press.

Flowers, R.M. & Kelley, S.A. 2011. Interpreting data dispersion and ‘ inverted’ dates in apatite (U-Th)/He and fission-track datasets: An example from the US midcontinent. *Geochimica et Cosmochimica Acta*, **75**, 5169–5186, https://doi.org/10.1016/j.gca.2011.06.016.

Flowers, R.M., Shuster, D.L., Wernicke, B.P. & Farley, K.A. 2007. Radiation damage control on apatite (U-Th)/He dates from the Grand Canyon region, Colorado Plateau. *Geology*, **35**, 447, https://doi.org/10.1130/G23471A.1.

Flowers, R.M., Ketcham, R.A., Shuster, D.L. & Farley, K.A. 2009. Apatite (U-Th)/He thermochronometry using a radiation damage accumulation and annealing model. *Geochimica et Cosmochimica Acta*, **73**, 2347–2365, https://doi.org/10.1016/j.gca.2009.01.015.

Galbraith, R.F. 1981. On statistical models for fission track counts. *Journal of the International Association for Mathematical Geology*, **13**, 471–478, https://doi.org/10.1007/BF01034498.

Galbraith, R.F. & Green, P.F. 1990. Estimating the component ages in a finite mixture. *International Journal of Radiation Applications and Instrumentation. Part D. Nuclear Tracks and Radiation Measurements*, **17**, 197–206, https://doi.org/10.1016/1359-0189(90)90035-V.

Galbraith, R.F., Laslett, G.M., Green, P.F. & Duddy, I.R. 1990. Apatite fission track analysis: geological thermal history analysis based on a three-dimensional random process of linear radiation damage. *Philosophical Transactions of the Royal Society of London. Series A: Physical and Engineering Sciences*, **332**, 419–438, https://doi.org/10.1098/rsta.1990.0124.

Gallagher, K. 2012. Transdimensional inverse thermal history modeling for quantitative thermochronology. *Journal of Geophysical Research: Solid Earth*, **117**, 1–16, https://doi.org/10.1029/2011JB008825.

Gallagher, K. & Brown, R. 1997. The onshore record of passive margin evolution. *Journal of the Geological Society*, **154**, 451–457, https://doi.org/10.1144/gsjgs.154.3.0451.

Gallagher, K. & Brown, R.W. 1999. The Mesozoic denudation history of the Atlantic margins of southern Africa and southeast Brazil and the relationship to offshore sedimentation. *Geological Society, London, Special Publications*, **153**, 41–53, https://doi.org/10.1144/GSL.SP.1999.153.01.03.

Gallagher, K., Hawkesworth, C.J. & Mantovani, M.S.M. 1994. The denudation history of the onshore continental margin of SE Brazil inferred from apatite fission track data. *Journal of Geophysical Research: Solid Earth*, **99**, 18117–18145, https://doi.org/10.1029/94JB00661.

Gallagher, K., Hawkesworth, C.J. & Mantovani, M.S.M. 1995. Denudation, fission track analysis and the long-term evolution of passive margin topography: application to the southeast Brazilian margin. *Journal of South American Earth Sciences*, **8**, 65–77, https://doi.org/10.1016/0895-9811(94)00042-Z.

Gallagher, K., Charvin, K., Nielsen, S., Sambridge, M. & Stephenson, J. 2009. Markov chain Monte Carlo (MCMC) sampling methods to determine optimal models , model resolution and model choice for Earth Science problems. *Marine and Petroleum Geology*, **26**, 525–535, https://doi.org/10.1016/j.marpetgeo.2009.01.003.

Gaucher, C., 2000. Sedimentology, palaeontology and stratigraphy of the Arroyo del Soldado Group (Vendian to Cambrian, Uruguay). Beringeria 26, 1-120.

Gaucher, C., Babinski, M., Blanco, G. 2016. Riolitas del Cretácico Superior (Campaniense); el magmatismo más joven de Uruguay. In: VIII Congreso Uruguayo de Geología, Actas, pp. 160-161, Montevideo.

Gaucher, C., Bossi, J., Blanco, G., 2009a. Palaeogeography. Neoproterozoic-Cambrian evolution of the Río de la Plata Palaeocontinent. In: Gaucher, C., Sial, A.N., Halverson, G.P., Frimmel, H.E. (Eds): Neoproterozoic-Cambrian Tectonics, Global Change and Evolution: a focus on southwestern Gondwana. Developments in Precambrian Geology, 16, Elsevier, pp. 131-141 .

Gaucher, C., Bossi, J., Samaniego, L., Frei, R., 2014a. Complejo Tapes. *In: Bossi, J., Gaucher, C. (Eds.) Geología del Uruguay. Tomo 1: Predevónico. Polo, Montevideo, pp. 253-264.*

Gaucher, C., Finney, S.C., Poiré, D.G., Valencia, V.A., Grove, M., Blanco, G., Pamoukaghlián, K., Gómez Peral, L., 2008. Detrital zircon ages of Neoproterozoic sedimentary successions in Uruguay and Argentina: insights into the geological evolution of the Río de la Plata Craton. Precambrian Research 167, 150-170.

Gaucher, C., Frei, R., Sial, A.N., Castiglioni, E., Ferreira, V.P., 2014b. Grupo Cebollatí. *In: Bossi, J., Gaucher, C. (Eds.) Geología del Uruguay. Tomo 1: Predevónico. Polo, Montevideo, pp. 155-169.*

Gaucher, C.; Frimmel, H.E., Germs, G.J.B. 2009b. Tectonic events and palaeogeographic evolution of southwestern Gondwana in the Neoproterozoic and Cambrian. In: *Gaucher, C., Sial, A.N., Halverson, G.P., Frimmel, H.E. (Eds): Neoproterozoic-Cambrian Tectonics, Global Change and Evolution: a focus on southwestern Gondwana. Developments in Precambrian Geology, 16, Elsevier, pp. 295-316.*

Gaucher, C., Nóbrega Sial, A., Blanco, G. & Sprechmann, P. 2004. Chemostratigraphy of the lower Arroyo del soldado group (Vendian, Uruguay) and palaeoclimatic implications. *Gondwana Research*, **7**, 715–730, https://doi.org/10.1016/S1342-937X(05)71058-3.

Gaucher, C., Chemale, F., Bossi, J. & Castiglioni, E.A. 2010. Grupo Cebollattí, Tererno Nico Perez: definición y edad. *VI Congreso Uruguayo de Geología, Minas*.

Gaucher, C., Frei, R., et al. 2011. Mesoproterozoic evolution of the Río de la Plata Craton in Uruguay: At the heart of Rodinia? *International Journal of Earth Sciences*, **100**, 273–

288, https://doi.org/10.1007/s00531-010-0562-x.

Gibson, S.A., Thompson, R.N. & Day, J.A. 2006. Timescales and mechanisms of plume-lithosphere interactions: 40Ar/39Ar geochronology and geochemistry of alkaline igneous rocks from the Paraná-Etendeka large igneous province. *Earth and Planetary Science Letters*, **251**, 1–17, https://doi.org/10.1016/j.epsl.2006.08.004.

Gleadow, A.J.W. 1981. Fission-track dating methods: What are the real alternatives? *Nuclear Tracks*, **5**, 3–14, https://doi.org/10.1016/0191-278X(81)90021-4.

Gleadow, A.J.W., Duddy, I.R., Green, P.F. & Lovering, J.F. 1986a. Confined fission track lengths in apatite: a diagnostic tool for thermal history analysis. *Contributions to Mineralogy and Petrology*, **94**, 405–415, https://doi.org/10.1007/BF00376334.

Gleadow, A.J.W., Duddy, I.R., Green, P.F. & Hegarty, K.A. 1986b. Fission track lengths in the apatite annealing zone and the interpretation of mixed ages. *Earth and Planetary Science Letters*, **78**, 245–254, https://doi.org/10.1016/0012-821X(86)90065-8.

Gomes, C.H. & Almeida, D. 2019. New insights into the Gondwana breakup at the Southern South America by apatite fission-track analyses. *Advances in Geosciences*, **47**, 1–15, https://doi.org/10.5194/adgeo-47-1-2019.

Granot, R. & Dyment, J. 2015. The Cretaceous opening of the South Atlantic Ocean. *Earth and Planetary Science Letters*, **414**, 156–163, https://doi.org/10.1016/j.epsl.2015.01.015.

Green, P.F. 1986. On the thermo-tectonic evolution of Northern England: Evidence from fission track analysis. *Geological Magazine*, **123**, 493–506, https://doi.org/10.1017/S0016756800035081.

Green, P.F. & Duddy, I.R. 2006. Interpretation of apatite (U–Th)/He ages and fission track ages from cratons. *Earth and Planetary Science Letters*, **244**, 541–547, https://doi.org/10.1016/j.epsl.2006.02.024.

Guenthner, W.R., Reiners, P.W., Ketcham, R.A., Nasdala, L. & Giester, G. 2013. Helium diffusion in natural zircon: radiation damage, anisotropy, and the interpretation of zircon (U-TH)/He thermochronology. *American Journal of Science*, **313**, 145–198, https://doi.org/10.2475/03.2013.01.

Hackspacher, P.C., Ribeiro, L.F.B., Ribeiro, M.C.S., Fetter, A.H., Hadler Neto, J.C., Tello, C.E.S. & Dantas, E.L. 2004. Consolidation and break-up of the South American Platform in southeastern Brazil: Tectonothermal and denudation histories. *Gondwana Research*, **7**, 91–101, https://doi.org/10.1016/S1342-937X(05)70308-7.

Hartmann, L.A., Campal, N., Santos, J.O.S., McNaughton, N.J., Bossi, J., Schipilov, A. & Lafon, J.M. 2001. Archean crust in the Rio de la Plata Craton, Uruguay - SHRIMP U-Pb zircon reconnaissance geochronology. *Journal of South American Earth Sciences*, **14**, 557–570, https://doi.org/10.1016/S0895-9811(01)00055-4.

Hartmann, L.A., Santos, J.O.S., Cingolani, C.A., McNaughton, N.J. 2002. Two Paleoproterozoic Orogenies in the Evolution of the Tandilia Belt, Buenos Aires, as evidenced by zircon U-Pb SHRIMP geochronology. International Geology Review, 44: 528-543.

Hueck, M., Oriolo, S., et al. 2017. Phanerozoic low-temperature evolution of the Uruguayan Shield along the South American passive margin. *Journal of the Geological Society of London*, https://doi.org/10.1144/jgs2016-101.

Hueck, M., Dunkl, I., Heller, B., Angelo, M., Basei, S. & Siegesmund, S. 2018a. (U-Th)/ He Thermochronology and Zircon Radiation Damage in the South American Passive Margin : Thermal Overprint of the Paraná LIP ? 1–18, https://doi.org/10.1029/2018TC005041.

Hueck, M., Oyhantçabal, P., Philipp, R.P., Angelo, M., Basei, S. & Siegesmund, S. 2018b. *The Dom Feliciano Belt in Southern Brazil and Uruguay*. Siegesmund, S., Basei, M. A. S., Oyhantçabal, P. & Oriolo, S. (eds). Cham, Springer International Publishing, Regional Geology Reviews, https://doi.org/10.1007/978-3-319-68920-3.

Hurford, A.J. 1990. Standardization of Fission-Track Dating Calibration - Recommendation by the Fission-Track Working Group of the Iugs Subcommission on Geochronology. *Chemical Geology*, **80**, 171-178 ST-Standardization of Fission-Track Dat.

Hurford, A.J. & Green, P.F. 1983. The zeta age calibration of fission-track dating. *Chemical Geology*, **41**, 285–317, https://doi.org/10.1016/S0009-2541(83)80026-6.

Jelinek, A.R., Cezar, A., Neto, B. & Poupeau, G. 2003. Análise Por Traços De Fissão Em Apatitas Do Distrito Fluorítico De Santa Catarina : Relações Entre Hidrotermalismo E Evolução Da Margem Continental. *Recherche*, **33**, 289–298.

Jonckheere, R. 2003. On methodical problems in estimating geological temperature and time from measurements of fission tracks in apatite. *Radiation Measurements*, **36**, 43–55, https://doi.org/10.1016/S1350-4487(03)00096-9.

Karl, M., Glasmacher, U.A., Kollenz, S., Franco-Magalhaes, A.O.B., Stockli, D.F. & Hackspacher, P.C. 2013. Evolution of the South Atlantic passive continental margin in southern Brazil derived from zircon and apatite (U-Th-Sm)/He and fission-track data. *Tectonophysics*, **604**, 224–244, https://doi.org/10.1016/j.tecto.2013.06.017.

Ketcham, R.A. 2005. Forward and Inverse Modeling of Low-Temperature Thermochronometry Data. *Reviews in Mineralogy and Geochemistry*, **58**, 275–314, https://doi.org/10.2138/rmg.2005.58.11.

Ketcham, R.A., Donelick, R.A. & Donelick, M.B. 2000. AFTSolve: A program for multi-kinetic modeling of apatite fission-track data. *American Mineralogist*, **88**, 929.

Ketcham, R.A., Carter, A., Donelick, R.A., Barbarand, J. & Hurford, A.J. 2007. Improved modeling of fission-track annealing in apatite. *American Mineralogist*, **92**, 799–810, https://doi.org/10.2138/am.2007.2281.

Kollenz, S. 2015. *Long-Term Landscape Evolution, Cooling and Exhumation History of the*

South American Passive Continental Margin in NE Argentina & SW Uruguay.

Kollenz, S., Glasmacher, U.A., Rossello, E.A., Stockli, D.F., Schad, S. & Pereyra, R.E. 2017. Thermochronological constraints on the Cambrian to recent geological evolution of the Argentina passive continental margin. *Tectonophysics*, **716**, 182–203, https://doi.org/10.1016/j.tecto.2016.11.019.

Krob, F.C., Glasmacher, U.A., Karl, M., Perner, M., Hackspacher, P.C. & Stockli, D.F. 2019. Multi-chronometer thermochronological modelling of the Late Neoproterozoic to recent t-T-evolution of the SE coastal region of Brazil. *Journal of South American Earth Sciences*, **92**, 77–94, https://doi.org/10.1016/j.jsames.2019.02.012.

Lal, D., Rajan, R.S. & Tamhane, A.S. 1969. Chemical Composition of Nuclei of Z > 22 in Cosmic Rays using Meteoritic Minerals as Detectors. *Nature*, **211**, 33–37, https://doi.org/10.1038/221033a0.

Machado, J.P.S.L., Jelinek, A.R., Bicca, M.M., Stephenson, R. & Genezini, F.A. 2019. West Gondwana orogenies and Pangaea breakup: thermotectonic effects on the southernmost Mantiqueira Province, Brazil. *Journal of the Geological Society*, jgs2019-018, https://doi.org/10.1144/jgs2019-018.

Mallmann, G., Chemale, F., Ávila, J.N., Kawashita, K. & Armstrong, R.A. 2007. Isotope geochemistry and geochronology of the Nico Pérez Terrane, Rio de la Plata Craton, Uruguay. *Gondwana Research*, **12**, 489–508, https://doi.org/10.1016/j.gr.2007.01.002.

Masquelin, H. 2006. El Escudo Uruguayo. *In*: *Cuencas Sedimentarias Del Uruguay*. DIRAC Facultad de Ciencias, 37–106.

Meisling, K.E., Cobbold, P.R. & Mount, V.S. 2001. Segmentation of an obliquely rifted margin, Campos and Santos basins, southeastern Brazil. *AAPG Bulletin*, **85**, 1903–1924, https://doi.org/10.1306/8626D0B3-173B-11D7-8645000102C1865D.

Milani, E.J. 1997. *Evolução Tectono-Estratigráfica Da Bacia Do Paraná e Seu*

Relacionamento Com a Geodinâmica Fanerozóica Do Gondwana Sul-Ocidental. Universidade Federal do Rio Grande do Sul.

Milani, E.J. & Wit, M.J. De. 2008. Correlations between the classic Paraná and Cape − Karoo sequences of South America and southern Africa and their basin infills flanking the Gondwanides : du Toit revisited ′ and Cape – Karoo Correlations between the classic Parana sequences of South Amer, https://doi.org/10.1144/SP294.17.

Milani, E.J., Melo, J.H.G. de, Souza, P.A. De, Fernandes, L.A. & França, A.B. 2007. Bacia do Paraná. *Boletim de Geociências da Petrobras*, **8**, 265–287.

Morales, E., Chang, H.K., et al. 2017. Tectonic and stratigraphic evolution of the Punta del Este and Pelotas basins (offshore Uruguay). *Petroleum Geoscience*, **23**, 415–426, https://doi.org/10.1144/petgeo2016-059.

Murray, K.E., Orme, D.A. & Reiners, P.W. 2014. Effects of U–Th-rich grain boundary phases on apatite helium ages. *Chemical Geology*, **390**, 135–151, https://doi.org/10.1016/j.chemgeo.2014.09.023.

Nasdala, L., Reiners, P.W., Garver, J.I., Kennedy, A.K., Stern, R.A., Balan, E. & Wirth, R. 2004. Incomplete retention of radiation damage in zircon from Sri Lanka. *American Mineralogist*, **89**, 219–231, https://doi.org/10.2138/am-2004-0126.

Oliveira, C.H.E. de, Jelinek, A.R., Chemale, F. & Bernet, M. 2016. Evidence of post-Gondwana breakup in Southern Brazilian Shield: Insights from apatite and zircon fission track thermochronology. *Tectonophysics*, **666**, 173–187, https://doi.org/10.1016/j.tecto.2015.11.005.

Oriolo, S., Oyhantçabal, P., Basei, M.A.S., Wemmer, K. & Siegesmund, S. 2016a. The Nico Pérez Terrane (Uruguay): From Archean crustal growth and connections with the Congo Craton to late Neoproterozoic accretion to the Río de la Plata Craton. *Precambrian Research*, **280**, 147–160, https://doi.org/10.1016/j.precamres.2016.04.014.

Oriolo, S., Oyhantçabal, P., et al. 2016b. Timing of deformation in the Sarandí del Yí Shear Zone, Uruguay: Implications for the amalgamation of western Gondwana during the Neoproterozoic Brasiliano-Pan-African Orogeny. *Tectonics*, **35**, 754–771, https://doi.org/10.1002/2015TC004052.

Oriolo, S., Hueck, M., Oyhantçabal, P., Goscombe, B., Wemmer, K. & Siegesmund, S. 2018. Shear Zones in Brasiliano-Pan-African Belts and Their Role in the Amalgamation and Break-Up of Southwest Gondwana. *In*: *Geology of Southwest Gondwana*. Springer International Publishing, 593–613., https://doi.org/10.1007/978-3-319-68920-3.

Oyhantçabal, P., Siegesmund, S. & Wemmer, K. 2011. The Río de la Plata Craton: A review of units, boundaries, ages and isotopic signature. *International Journal of Earth Sciences*, **100**, 201–220, https://doi.org/10.1007/s00531-010-0580-8.

Oyhantçabal, P.B., Wagner-Eimer, M., Wemmer, K., Schulz, B., Frei, R., Siegesmund, S., 2012. Paleo- and Neoproterozoic magmatic and tectonometamorphic evolution of the Isla Cristalina de Rivera (Nico Pérez Terrane, Uruguay). International Journal of Earth Sciences 101, 1745-1762.

Oyhantçabal, P., Cingolani, C.A. & Wemmer, K. 2018. *The Río de La Plata Craton of Argentina and Uruguay*. Springer International Publishing, https://doi.org/10.1007/978-3-319-68920-3.

Pamoukaghlián, K., Gaucher, C., Frei, R., Poiré, D. G., Chemale, F., Frei, D., Will, T. M., 2017. U-Pb age constraints for the La Tuna Granite and Montevideo Formation (Paleoproterozoic, Uruguay): Unravelling the structure of the Río de la Plata Craton. Journal of South American Earth Sciences 79, 443-458.

Panario, D., Gutierrez, O., Bettucci, L.S., Peel, E., Oyhantçabal, P. & Raba. 2014. Ancient Landscapes of Uruguay. *In*: *Gondwana Landscapes in Southern South America: Argentina, Uruguay and Southern Brazil*. 1–545., https://doi.org/10.1007/978-94-007-

7702-6.

Pankhurst, R.J., Rapela, C.W., Fanning, C.M. & Márquez, M. 2006. Gondwanide continental collision and the origin of Patagonia. *Earth-Science Reviews*, **76**, 235–257, https://doi.org/10.1016/j.earscirev.2006.02.001.

Peel, E., Sánchez Bettucci, L., Basei, M.A.S., 2018. Geology and geochronology of Paso del Dragón Complex (northeastern Uruguay): implications on the evolution of the Dom Feliciano Belt (Western Gondwana). J. South Amer. Earth Sci. 85, 250-262.

Philipp, R.P., Pimentel, M.M. & Chemale, F. 2016. Tectonic evolution of the Dom Feliciano Belt in Southern Brazil: Geological relationships and U-Pb geochronology. *Brazilian Journal of Geology*, **46**, 83–104, https://doi.org/10.1590/2317-4889201620150016.

Philipp, R.P., Pimentel, M.M. & Basei, M.A.S. 2018. The Tectonic Evolution of the São Gabriel Terrane, Dom Feliciano Belt, Southern Brazil: The Closure of the Charrua Ocean. *In*: *Geology of Southwest Gondwana*. Springer International Publishing, 243–265., https://doi.org/10.1007/978-3-319-68920-3.

Price, P.B. & Walker, R.M. 1963. Fossil tracks of charged particles in mica and the age of minerals. *Journal of Geophysical Research*, **68**, 4847–4862, https://doi.org/10.1029/JZ068i016p04847.

Quirk, D.G. & Rüpke, L.H. 2018. Melt-induced buoyancy may explain the elevated rift-rapid sag paradox during breakup of continental plates. *Scientific Reports*, **8**, 1–13, https://doi.org/10.1038/s41598-018-27981-2.

Rapela, C.W., Fanning, C.M., Casquet, C., Pankhurst, R.J., Spalletti, L., Poiré, D. & Baldo, E.G. 2011. The Rio de la Plata craton and the adjoining Pan-African/brasiliano terranes: Their origins and incorporation into south-west Gondwana. *Gondwana Research*, **20**, 673–690, https://doi.org/10.1016/j.gr.2011.05.001.

Reiners, P.W. 2005. Zircon (U-Th)/He Thermochronometry. *In*: *Reviews in Mineralogy and*

Geochemistry. 151–179., https://doi.org/10.2138/rmg.2005.58.6.

Reiners, P.W. & Farley, K.A. 2001. Influence of crystal size on apatite (U-Th)/He thermochronology: An example from the Bighorn Mountains, Wyoming. *Earth and Planetary Science Letters*, **188**, 413–420, https://doi.org/10.1016/S0012-821X(01)00341-7.

Reiners, P.W., Farley, K.A. & Hickes, H.J. 2002. He diffusion and (U-Th)/He thermochronometry of zircon: Initial results from Fish Canyon Tuff and Gold Butte. *Tectonophysics*, **349**, 297–308, https://doi.org/10.1016/S0040-1951(02)00058-6.

Reiners, P.W., Spell, T.L., Nicolescu, S. & Zanetti, K.A. 2004. Zircon (U-Th)/He thermochronometry: He diffusion and comparisons with 40Ar/39Ar dating. *Geochimica et Cosmochimica Acta*, **68**, 1857–1887, https://doi.org/10.1016/j.gca.2003.10.021.

Reiners, P.W., Carlson, R.W., Renne, P.R., Cooper, K.M., Granger, D.E., McLean, N.M. & Schoene, B. 2018. The (U-Th)He system. *In*: *Geochronology and Thermochronology*. John Wiley & Sons Ltd., 291–363.

Ribot, A., Bossi, J., Cingolani, C.A., Piñeyro, D. 2005. Caracterización petrográfica de la faja milonítica Colonia-Arroyo Pavón en el Sur del Terreno Piedra Alta, Uruguay: Zona de cizalla principal en basamento precámbrico? Actas 16º Congreso Geológico Argentino, 789, La Plata.

Reuber, K., Mann, P. & Pindell, J. 2019. Hotspot Origin for Asymmetrical Conjugate Volcanic Margins of the Austral South Atlantic Ocean As Imaged on Deeply-Penetrating Seismic Reflection Images. *Interpretation*, 1–88, https://doi.org/10.1190/int-2018-0256.1.

Rossello, E.A., De Santa Ana, H. & Veroslavsky, G. 2000. El lineamiento Santa Lucia-Aigua-Merin (Uruguay): un corredor tectonico extensivo y transcurrente dextral precursos de la apertura atlantica. *Revista Brasileira de Geociências*, **30**, 749–756.

Rossello, E.A., Veroslavsky, G., Masquelin, H. & De Santa Ana, H. 2007. El corredor juro-cretácico Santa Lucía-Aiguá-Merín (Uruguay): Evidencias cinemática transcurrente dextral y controles preexistentes. *Revista de la Asociacion Geologica Argentina*, **62**, 92–104.

Rossetti, L.M., Lima, E.F., Waichel, B.L., Scherer, C.M. & Barreto, C.J. 2014. Stratigraphical framework of basaltic lavas in Torres Syncline main valley, southern Parana-Etendeka Volcanic Province. *Journal of South American Earth Sciences*, **56**, 409–421, https://doi.org/10.1016/j.jsames.2014.09.025.

Santos, J.OS., Hartmann, L.A., Bossi, J., Campal, N., Schipilov, A., Piñeyro, D., McNaughton, N.J., 2003. Duration of the Transamazonian and its correlation within South America based on U-Pb SHRIMP geochronology of the la Plata Craton, Uruguay. International Geology Review 45, 27-48.

Santos, J. O., Chernicoff, C. J., Zappettini, E. O., McNaughton, N. J., Greau, Y. 2017. U-Pb geochronology of Martín García, Sola, and Dos Hermanas Islands (Argentina and Uruguay): Unveiling Rhyacian, Statherian, Ectasian, and Stenian of a forgotten area of the Río de la Plata Craton. Journal of South American Earth Sciences, 80, 207-228.

Schmitt, R. da S., Fragoso, R.D.A. & Collins, A.S. 2018. Suturing Gondwana in the Cambrian: The Orogenic Events of the Final Amalgamation. *In*: *Geology of Southwest Gondwana*. Springer International Publishing, 411–432., https://doi.org/10.1007/978-3-319-68920-3_15.

Scotese, C.R., Boucot, A.J. & McKerrow, W.S. 1999. Gondwanan palaeogeography and palaeoclimatology. *Journal of African Earth Sciences*, **28**, 99–114.

Shuster, D.L., Flowers, R.M. & Farley, K.A. 2006. The influence of natural radiation damage on helium diffusion kinetics in apatite. *Earth and Planetary Science Letters*, **249**, 148–161, https://doi.org/10.1016/j.epsl.2006.07.028.

Soto, M., Morales, E., Veroslavsky, G., de Santa Ana, H., Ucha, N. & Rodríguez, P. 2011. The continental margin of uruguay: Crustal architecture and segmentation. *Marine and Petroleum Geology*, **28**, 1676–1689, https://doi.org/10.1016/j.marpetgeo.2011.07.001.

Sprechmann, P., Bossi, J., Da Silva, J. 1981. Cuencas del Jurásico y Cretácico del Uruguay. In: Volkheimer, W., Musacchio (Eds.) Cuencas sedimentarias del Jurásico y Cretácico de América del Sur, 1, pp. 239-270, Buenos Aires.

Sprechmann, P., Montaña, J., Gaucher, C. 1993. Devónico. In: Bossi, J. (Ed.): Geología y Recursos Minerales del Departamento de Durazno. Intendencia Municipal de Durazno y Cátedra de Geología de la Facultad de Agonomía, Montevideo, pp. 25-55.

Stockli, D.F. 2005. Application of low-temperature thermochronometry to extensional tectonic settings. *In*: Reiners, P. W. & Ehlers, T. A. (eds) *Low-Temperature Thermochronology: Techniques, Interpretations, and Applicationscations*. Mineralogical Society of America, 411–448.

Stockli, D.F., Farley, K.A. & Dumitru, T.A. 2000. Calibration of the apatite (U-Th)/ He thermochronometer on an exhumed fault block , White Mountains , California. *Geology*, **28**, 983–986, https://doi.org/10.1130/0091-7613(2000)28<983.

Tagami, T. & O'Sullivan, P.B. 2005. Fundamentals of fission-track thermochronology. *In*: Reiners, P. W. & Ehlers, T. A. (eds) *Low-Temperature Thermochronology: Techniques, Interpretations, and Applications*. Mineralogical Society of America, 19–48.

Teixeira W., Renne, P., Bossi. J., Campal, N., D'Agrella, F., 1999. ^{40}Ar/^{39}Ar and Rb/Sr geochronology of the Uruguayan dike swarm, Río de la Plata Craton and implications for Proterozoic intraplate activity in western Gondwana. Precambrian Research, 93, 153-180.

Tello Saenz, C.A., Hackspacher, P.C., et al. 2003. Recognition of Cretaceous, Paleocene, and Neogene tectonic reactivation through apatite fission-track analysis in Precambrian areas of southeast Brazil: association with the opening of the south Atlantic Ocean. *Journal of South American Earth Sciences*, **15**, 765–774, https://doi.org/10.1016/S0895-9811(02)00131-1.

Turner, S., Regelous, M., et al. 1994. Magmatism and Continental Break-Up in the South Atlantic. *Earth. Planet. Sci. Lett.*, **121**, 333–348, https://doi.org/10.1016/0012-821X(94)90076-0.

Uriz, N.J., Cingolani, C.A., Basei, M.A.S., Blanco, G., Abre, P., Portillo, N.S. & Siccardi, A. 2016. Provenance and paleogeography of the Devonian Durazno Group, southern Parana Basin in Uruguay. *Journal of South American Earth Sciences*, **66**, 248–267, https://doi.org/10.1016/j.jsames.2016.01.002.

Van Ranst, G., Pedrosa-Soares, A.C., Novo, T., Vermeesch, P. & De Grave, J. 2019. New insights from low-temperature thermochronology into the tectonic and geomorphologic evolution of the south-eastern Brazilian highlands and passive margin. *Geoscience Frontiers*, https://doi.org/10.1016/j.gsf.2019.05.011.

Vermeesch, P. 2009. RadialPlotter: a Java application for fission track, luminescence and other radial plots. *Radiation Measurementes*, 409–410http://www.ucl.ac.uk/~ucfbpve/radialplotter/.

Veroslavsky, G., De Santa Ana, H., Rossello, E. 2004. Depósitos del Jurásico y Cretácico temprano de la región meridional de Uruguay. In: Veroslavsky, G., Ubilla, M., Martínez, S. (Eds.): Cuencas sedimentarias de Uruguay. Mesozoico. Facultad de Ciencias, Montevideo, pp. 117-142.

Wagner, G.A., Gleadow, A.J.W. & Fitzgerald, P.G. 1989. The significance of the partial annealing zone in apatite fission-track analysis: Projected track length measurements and uplift chronology of the transantarctic mountains. *Chemical Geology: Isotope Geoscience section*, **79**, 295–305, https://doi.org/10.1016/0168-9622(89)90035-3.

Will, T.M. & Frimmel, H.E. 2018. Where does a continent prefer to break up? Some lessons from the South Atlantic margins. *Gondwana Research*, **53**, 9–19, https://doi.org/10.1016/j.gr.2017.04.014.

Will, T. , Gaucher, C., Ling, X.X. , Li, X.H. , Li, Q.L. , Frimmel, H.E. 2019 Neoproterozoic magmatic and metamorphic events in the Cuchilla Dionisio Terrane, Uruguay, and possible correlations across the South Atlantic. Precambrian Research 320, 303-322.

Wolf, R.A., Farley, K.A. & Silver, L.T. 1996. Helium diffusion and low-temperature thermochronometry of apatite. *Geochimica et Cosmochimica Acta*, **60**, 4231–4240, https://doi.org/10.1016/S0016-7037(96)00192-5.

Wolf, R.A., Farley, K.A. & Kass, D.M. 1998. Modeling of the temperature sensitivity of the apatite (U-Th)/He thermochronometer. *Chemical Geology*, **148**, 105–114, https://doi.org/10.1016/S0009-2541(98)00024-2.

Zalán, P. V. 2004. Evolução Fanerozóica das Bacias Sedimentares Brasileiras. *In*: Mantesso-Neto, V., Bartorelli, A., Carneiro, C. D. R. & Neves, B. B. de B. (eds) *Geologia Do Continente Sul-Americano: Evolução Da Obra de Fernando Flávio Marques de Almeida*. Beca Produções Culturais Ltda, 595–612.

Zambrano, J.J. & Urien, C.M. 1970. Geological outline of the basins in southern Argentina and their continuation off the Atlantic shore. *Journal of Geophysical Research*, **75**, 1363–1396, https://doi.org/10.1029/JB075i008p01363.

Zerfass, H., Chemale, F., Leandro, C. & Lavina, E. 2004. Tectonics and sedimentation in Southern South America during Triassic. **166**, 265–292, https://doi.org/10.1016/j.sedgeo.2003.12.008.